J. Membrane Biol. 158, 31–48 (1997)

The Journal of
Membrane
Biology

Caco-2 Cell Line Used as an *In Vitro* Model to Study Cadmium Accumulation in Intestinal Epithelial Cells

C. Jumarie[1], P.G.C. Campbell[2], A. Berteloot[3], M. Houde[4], F. Denizeau[1]

[1]Département de Chimie, Université du Québec à Montréal, C.P. 8888, Succ. Centre-Ville, Montreal, Quebec H3C 3P8, Canada
[2]INRS-Eau, INRS, Université du Québec, Ste-Foy, Canada
[3]GRTM, département de Physiologie, Université de Montréal, Montreal, Canada
[4]Département des Sciences Biologiques, Université du Québec à Montréal, Montreal, Canada

Received: 19 January 1996/Revised: 23 January 1997

Abstract. ^{109}Cd uptake was studied using the highly differentiated TC7 clone of Caco-2 cells as a model of human enterocyte function. Intracellular accumulation of 0.3 μM ^{109}Cd involved a rapid and a slow uptake phase, which resulted in complete equilibration ($t_{1/2}$ = 17.3 ± 1.3 min) with an apparent in-to-out distribution ratio (α_e) of 11.6 ± 0.8. The amplitude of the rapid phase (U_0) and the rate of the slow phase (V) were similarly reduced in the less differentiated PF11 clone, but comparable α_e values were observed at equilibrium. In both clones, the $t_{1/2}$ and α_e values increased and decreased, respectively, upon addition of unlabeled Cd to the uptake media. In TC7 cells, ^{109}Cd uptake at 1 min (U_1) was unaffected by Ca concentrations four order of magnitude in excess, but both U_0 and V demonstrated similar sensitivities to unlabeled Cd, Zn and sulfhydryl-reactive agents. Only U_0 disappeared when EDTA was present in the wash solutions. U_1 showed saturation kinetics and the data were found compatible with a model assuming rapid initial Cd binding and transport through a unique transport protein (K_m = 3.8 ± 0.7 μM). Cd efflux kinetics demonstrated partial reversibility in EDTA-containing solutions, suggesting that the taken up Cd might be both tightly and loosely bound to intracellular binding sites. However, the displacement of ^{109}Cd measured at 65 min failed to reveal this heterogeneity: the data were found compatible with a model equation assuming the presence of one class of high-capacity high-affinity binding sites. We conclude that a slow-transport fast-intracellular binding mechanism of Cd uptake best accounts for these results and that Cd transport most likely involves a carrier-type of protein unrelated to Ca absorption.

Key words: Cd transport — Kinetics, Caco-2 cell culture — Human enterocyte — Differentiation

Introduction

Cadmium (Cd) is a highly toxic metal with many industrial uses. Although attempts have been made to reduce Cd emissions during processing, the ubiquity of this metal as an environmental contaminant is well documented [33]. Cadmium enters the food chain, and both plants and animals can be contaminated. Following oral exposure, Cd is absorbed in mammals through the gastrointestinal tract and transported via the blood circulation to various tissues. The liver and kidneys are the major sites of Cd accumulation, and studies on Cd uptake and toxic effects have focused on these tissues [6, 16, 18]. Intestinal Cd absorption has been mainly investigated in terms of metabolism in humans [40] and rodents [20], but little is known about how Cd permeates the intestinal epithelial cells.

The most common hypothesis in the literature is that intestinal Cd uptake involves competition with essential elements such as Ca or Zn for specific transport systems, and most *in vivo* studies aimed at assessing Cd absorption have measured Cd body retention and Cd, Ca or Zn tissue distribution following oral Cd administration under different dietary Ca or Zn status [22, 27, 49]. Results obtained from such studies on Cd/Ca interactions in intestinal transport are however inconclusive: oral Cd administration was found either to inhibit Ca absorption [22, 43] or to be without significant effect [51]. Simi-

Correspondence to: F. Denizeau

larly, Cd was reported to decrease Zn absorption [42], but also to have the opposite effect [41]. Although *in vivo* studies certainly yield useful information about Cd metabolism and toxicity, they do not allow investigation of the membrane and cellular mechanisms responsible for Cd uptake and transport through the intestinal epithelium.

In parallel, *in vitro* approaches using perfused intestinal segments or everted gut sacs have provided mechanistic insights. Some studies have suggested that Cd may decrease basal and vitamin D-stimulated intestinal Ca absorption [4, 46], and both noncompetitive and competitive inhibitions have been proposed [23, 46]. Cadmium was shown to be a strong competitor of the intestinal Ca^{2+}-pumping ATPase responsible for ATP-driven Ca efflux across the basolateral membrane [48], but possible competition between Ca and Cd for intestinal uptake from the lumen through an apical transport system is still unclear. Similarly, the involvement of voltage-gated Ca channels in intestinal Cd uptake remains questionable since the existence of such channels in the enterocyte is not clearly established [47]. Moreover, Cd permeability through L-type Ca channels was reported to be extremely low relative to that of Ca [45], although some studies have shown that Cd may permeate membranes in part through these channels in liver [8] and kidney [12] cells. Techniques involving perfused intestinal segments have also provided data supporting the assumption that Cd competes with Zn for intestinal transport. Cadmium was shown to decrease Zn transport, but Cd transport to the vascular effluent was also found to increase upon Zn addition in the luminal perfusate [24]. Because of the heterogeneity of intestinal tissue itself, the nature of possible interactions remains unclear from these data. However, although Cd/Zn interactions were shown to be noncompetitive in such *in vitro* systems [15], strong competition was evident in brush border membrane vesicles isolated from the pig small intestine [44].

Because intestinal epithelial cells represent the first barrier to be crossed by Cd following oral administration, the mechanism of Cd absorption through these cells is of prime interest. In this context, human cell culture models are potentially useful for identifying cellular mechanisms. In the absence of differentiated normal intestinal cell lines, Caco-2 cells offer a valuable alternative. In fact, although derived from a human colon adenocarcinoma [13], these cells exhibit spontaneous enterocytic differentiation at confluency [35] and represent a particularly relevant *in vitro* model for studying human intestinal functions [7, 26, 38]. Moreover, the Caco-2 cell line has often been used as a model for studies of intestinal permeability to Ca [19] and to trace elements such as Fe [1] and Zn [36]. Finally, the recent isolation of Caco-2 cell clones showing either high or low levels of enterocytic differentiation [10] allows the study of intestinal functions in relation to differentiation status.

The aim of the present study was thus to characterize the kinetics of Cd uptake in the Caco-2 cell line used as a human enterocyte model under experimental conditions where Cd concentrations were comparable to what might be found in the bolus following the ingestion of contaminated foodstuffs [37]. The kinetic studies were performed in a minimal transport medium of defined composition, which allowed us to define and control Cd speciation in the extracellular environment. Our results clearly demonstrate that Cd uptake is a complex phenomenon to which contribute both specific and nonspecific transport and binding processes. The involvement of a Ca route is unlikely under our experimental conditions, but Cd uptake is highly sensitive to Zn inhibition and may involve a carrier-type of protein.

Materials and Methods

Cell Cultures

Caco-2 cells were obtained from the late Dr. J. Fogh (Sloan Kettering Institute for Cancer Research, Rye, NY) and were used between passages 80 and 90 (C#80–90). The PF11 and TC7 clones, which have been isolated from early and late passages of the Caco-2 cell line, respectively [10], were kindly supplied by Dr. A. Zweibaum (INSERM U178, Villejuif, France). Both clones were used between the 38th and 45th passages. Stock cultures were grown in 75 cm^2 plastic flasks in Dulbecco's Modified Eagle essential minimum medium (DMEM) containing 25 mM glucose and supplemented with 15% (C#80–90) or 20% (PF11 and TC7) inactivated fetal bovine serum (FBS), 0.1 mM nonessential amino acids and 50 units/ml penicillin +50 μg/ml streptomycin. Cultures were maintained at 37°C in a 5% CO_2—95% air atmosphere and were passaged weekly by trypsinization (0.05% trypsin/0.53 mM EDTA). For all experiments, cells were seeded in 35 × 10 mm Petri dishes at 40 × 10^3 (C#80–90), 20 × 10^3 (PF11) or 12 × 10^3 cells/cm^2 (TC7). With these specific seeding densities, cell confluence was achieved on day 6 in all cases. The medium was changed every 2 days, and the cultures were maintained for 18 days to reach the stationary growth phase and to allow maximal functional differentiation [10, 26].

Sucrase and Protein Assays

Cells from 6- or 18-day old cultures were collected from three Petri dishes and pooled for sucrase and protein assays. The culture plates were washed three times with 2 ml of ice-cold phosphate-buffered saline (PBS), pH 7.4. The cells were then carefully scraped off the plates with a rubber policeman and homogenized in cold PBS (3 plates/2 ml) by 1-min sonication (2.5 watts) using a Vibra Cell high intensity ultrasonic processor (Sonics & Materials). Samples were kept at −20°C for no longer than one week before analysis.

Sucrase activity (EC 3.2.1.48) was used as a marker of enterocytic differentiation and assayed at 37°C on cell homogenates according to the method of Kunst et al. [30] using a 28 mM sucrose concentration as described previously [25]. Protein content was determined

Table 1. Cd speciation in the transport medium

Name	% Total
$CdCl^+$	61.4
Cd^{2+}	14.0
$CdCl_2$	20.9
$CdCl_3^-$	1.8

The composition of the transport medium is described in the text. Cd speciation was calculated using the MINEQL$^+$ chemical equilibrium program. Species listed are those representing more than 1% of the total dissolved metal.

according to Bradford [9] using bovine serum albumin as the calibration standard.

Sucrase activity is expressed as milliunits per mg of protein (mU.mg protein^{-1}), one unit being defined as the activity which hydrolyses one μmol of substrate per min under the experimental conditions.

Cd Uptake Measurements

Cadmium uptake measurements were performed on 18-day-old cell cultures in a serum-free transport medium containing (in mM): 137 NaCl, 4.7 KCl, 1.2 KH_2PO_4, 1.2 $MgSO_4$, 2.5 $CaCl_2$, 4 D-glucose and 10 HEPES, buffered to pH 7.3 with 5 NaOH. Monolayers were washed four times with the Cd-free transport medium before incubation in 1 ml uptake medium containing 0.2 μCi (0.3 μM) of ^{109}Cd (sp. act. 0.665 mCi/μmol). Experimental media were always prepared in advance and allowed to equilibrate overnight at room temperature. The chemical forms of Cd at equilibrium in the transport medium were calculated using the MINEQL$^+$ chemical equilibrium program (Schecher, W., Westall. J., Environmental Research Software, copyright © 1994) and those species representing more than 1% of the total dissolved metal are listed in Table 1. In some cases, experiments were conducted in the presence of other metals or inhibitors. In all such examples, MINEQL$^+$ calculations were performed to verify that modifications to the transport medium did not induce any change in Cd speciation. Moreover, in inhibition experiments using 100 μM unlabeled Cd or different concentrations of Zn, each metal concentration was verified by atomic absorption spectrophotometric analysis [2], using a flame spectrophotometer (Varian, model Spectra-20). In all cases, metal concentration fell within the 90% confidence interval of the expected concentration.

All experiments were performed at room temperature (20°C–23°C) without agitation since uptake measurements performed on swirled or unswirled Petri dishes gave similar results (*data not shown*). Uptake was stopped by removing the transport medium and the monolayers were rapidly rinsed four times with 2 ml of ice-cold Cd-free transport medium to remove the excess radioactivity. In some experiments, these rinses were performed in Ca-, Mg-free medium containing 2 mM EDTA in order to extract the external labile metal fraction from the cell surface. Cells were then solubilized in 1N NaOH (0.5 ml) and aliquots of 300 μl were used for radioactivity determinations using a gamma counter (Compugamma CS, model 1282, Fisher Scientific Ltd.) whereas 50 μl of the remaining suspension was kept for protein assay.

Cd Efflux Measurements

Cadmium efflux measurements were performed at room temperature on 18-day-old cell monolayers. The cells were first exposed to 0.3 μM ^{109}Cd for 65 min, at which time uptake was stopped as described in the previous section, but using room temperature stop solution, before subsequent incubation in Cd-free medium for specific times. Efflux assays were stopped by removing the medium and the monolayers were rinsed four times with ice-cold stop solution. Cells were processed for radioactivity and protein determinations. In some experiments, both the washing procedures and the efflux measurements were performed in the presence of 2 mM EDTA (Ca-, Mg-free medium).

Data Analyses

Uptake Studies

The following notations consistently apply throughout the text.
U_0^* (pmol.mg protein^{-1}): zero-time intercept in time-course studies.
U_e^* (pmol.mg protein^{-1}): equilibrium Cd uptake estimated by nonlinear regression analyses of uptake data (U^*) obtained over the 0–65 min time range using Eq. (1),

$$U^* = U_e^* (1 - e^{-kt}) + U_0^* \quad (1)$$

or by the 65 min uptake values in Fig. 8.
k (min^{-1}): first-order rate constant of the uptake process estimated from Eq. (1).
V^* (pmol.min^{-1}.mg protein^{-1}): initial rate of Cd uptake measured by the slope of the linear regression analysis to uptake data obtained over the 0–60 sec or 0–3 min time ranges using Eq. (2).

$$U^* = V^* t + U_0^* \quad (2)$$

U_1^* (pmol.mg protein^{-1}): initial Cd uptake measured at a 1-min time point.
V_1^* (pmol.mg protein^{-1}): contribution of the slow uptake process during the initial phase to total uptake measured at 1 min. The numerical values of V_1^* and V^* are obviously similar when the latter are reported relative to a time scale in units of 1 min. The distinction between V_1^* and V^* was required to maintain a consistent set of units when assessing the contribution of V_1^* and U_0^* to U_1^*.
U_{1s}^*, U_{0s}^*, V_s^*, V_{1s}^*, U_{es}^*: specific fractions of the parameters defined above, respectively, which are inhibited by high concentrations of unlabeled Cd. Note that, in the above definitions, the superscript (*) indicates that Cd uptake values are expressed relative to pure concentrations of ^{109}Cd (this concentration was 0.3 μM in all experiments except those described in Fig. 6 where it was varied from 0.1 to 30 μM). The added unlabeled $CdCl_2$ thus acts as a pure competitive inhibitor of tracer Cd in these experiments.
S, T (μM): refer to unlabeled Cd and pure tracer ^{109}Cd concentrations, respectively. Indices (o) and (i) stand for the outside (incubation medium) and intracellular compartments, respectively.

All other notations are described in the text as necessary.

Cd Efflux Studies

Nonlinear regression analyses of the efflux (E^*) time-course data were performed using the first-order decay Eq. (3).

$$E^* = (E_0^* - E_e^*)\, e^{-k't} + E_e^* \quad (3)$$

in which E_0^* represents the amount of ^{109}Cd present in the cells at time $t = 0$ of efflux (and is thus equal to the sum of the U_0^* and U_e^* parameters defined in Eq. (1)) and E_e^* stands for the plateau of efflux reached with the first-order rate constant k'.

Kinetic Parameter Determinations

For the data reported in Figs. 6 and 8, the kinetic parameters were evaluated by nonlinear regression analyses as justified in the Results section. The maximum number of acceptable Michaelis-Menten terms in the equations used was determined through statistical evaluation of the successive curve-fittings according to the usual criteria [11].

The $t_{1/2}$ values reported in this paper represent the time for which tracer uptake or efflux was half-completed. Their numerical values were calculated using Eq. (4).

$$t_{1/2} = \frac{ln\ 2}{k \text{ or } k'} \tag{4}$$

in which the k and k' values were those estimated from Eqs. (1) and (3), respectively.

Both linear and nonlinear regression analyses were performed using the Enzfitter software (Robin J. Leatherbarrow, Copyright © 1987) and the robust weighting routine. The errors associated with the kinetic parameter values given in the text represent the standard errors of regression (SER). Where appropriate, the 95% confidence interval of the regressions was determined using Fig. P software (Biosoft Corporation, copyright © 1990).

MATERIALS

All culture ware (Falcon) was obtained from VWR Scientific (Toronto, Ont.) whereas DMEM, penicillin, streptomycin and trypsin were purchased from Gibco Laboratories (Grand Island, NY). FBS was obtained from Immunocorp (Montréal, Qué.) and was inactivated at 52°C for 30 min. Labeled $^{109}CdCl_2$ was obtained from Dupont Canada (Mississauga, Ont.) and cold $CdCl_2$ from Sigma Chemical (St-Louis, MO). $ZnCl_2$ was purchased from Anachemia (Lachine, Qué.) and $HgCl_2$ from Fisher Scientific Ltd. (Whitby, Ont.). Ouabain and *N*-ethylmaleimide (NEM) were obtained from Sigma Chemical, whereas parachloromercuribenzenesulfonate (pCMBS) was purchased from Aldrich Chemical (Milwaukee, WI). All salts and chemicals used for buffer preparation were of the highest purity available.

Results

KINETIC CHARACTERISTICS OF Cd UPTAKE IN CACO-2 CELLS IN RELATION TO THE CELL FUNCTIONAL DIFFERENTIATION STATUS

As shown in Fig. 1 from sucrase activity measurements in cell homogenates, confluent but undifferentiated 6-day-old cultures (open columns), all presented low levels of the specific brush border enzyme marker, and the lowest level was recorded in the PF11 clone. In contrast, sucrase activity was markedly increased in 18-day-old monolayers (dotted columns) originating from C#80–90 (54.6 ± 9.7 mU.mg protein^{-1}) and TC7 cells (117.4 ± 11.3 mU.mg protein^{-1}), but remained very low in the PF11 clone (21.6 ± 5.0 mU.mg protein^{-1}). These results agree quite closely with those of previous reports demonstrating that the enterocytic differentiation status of Caco-2 cells is a growth-related phenomenon [7, 26, 35], and that the TC7 and PF11 clones represent highly and

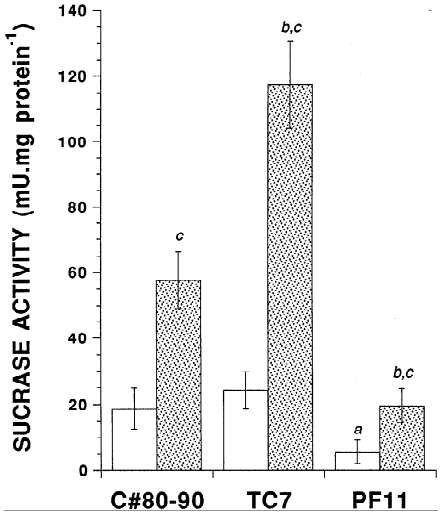

Fig. 1. Functional differentiation status of the different Caco-2 cells lines. Sucrase activity was measured as described in the text in cell homogenates from the parent Caco-2 cell line (C#80–90) and the TC7 and PF11 clones. Monolayers were maintained in culture for 6 (open columns) or 18 days (dotted columns). Values shown are means ± SEM evaluated on 5 different cell passages. Letters *a* and *b* indicate significant differences ($P \leq 0.05$) between values obtained, respectively, on days 6 and 18 in the clones relative to C#80–90, whereas letter *c* shows significant differences between values obtained on day 18 relative to day 6 for each cell line.

poorly differentiated phenotypes of enterocytelike cells, respectively, when compared to the parent cell line [10].

The time courses of 0.3 μM ^{109}Cd uptake recorded at different cell passages were highly reproducible for the three cell lines. The uptake kinetics could be well described by the first-order rate Eq. (1) under all experimental conditions and unlabeled Cd (30 μM) acted as an effective inhibitor of tracer uptake in all cell lines. These facts can be best appreciated for the TC7 and PF11 clones in Fig. 2, and for all cell lines in Table 2 summarizing the uptake parameter values. Taken together, these results demonstrate the general characteristics of Cd uptake in Caco-2 cells.

First, there is a major slow phase of Cd uptake that appears related to the cell functional differentiation status, the overall rate of Cd accumulation being significantly lower in the PF11 than in the TC7 cells (Fig. 2). This difference is reflected by the $t_{1/2}$ values shown in Table 2, which also indicates that the parent C#80–90 cells behave quite similarly to the cloned TC7 cells. Note in Table 2 that the $t_{1/2}$ values are also increased by a factor varying from 1.5– to 2.1–fold in all cell lines when the uptake assays are performed in the presence of 30 μM unlabeled Cd.

Second, there is a very rapid phase of Cd uptake that shows up as a non-zero intercept in the uptake time course (U_0^* parameter in Table 2), part of which should be considered as linked to the existence of a specific

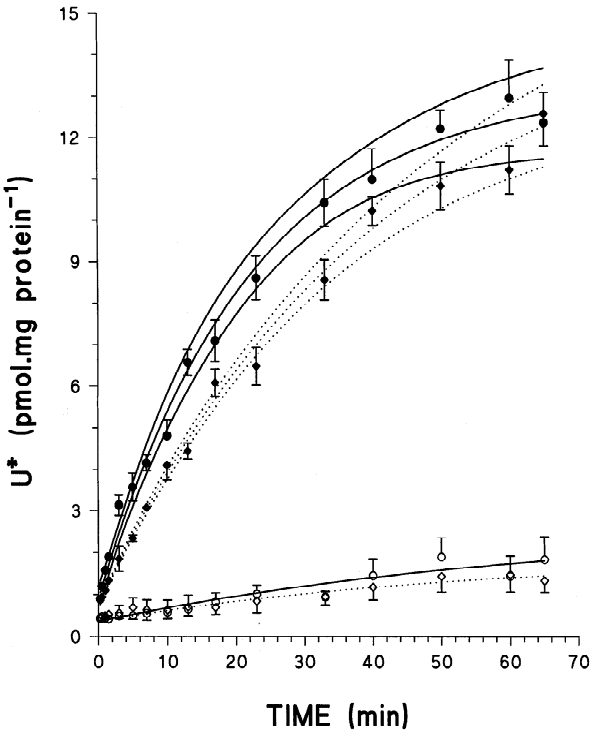

Fig. 2. Time course of 0.3 μM ^{109}Cd uptake (U*) in 18-day-old TC7 (circles) and PF11 (diamonds) cells. Uptake measurements were performed as described in the text in the absence (filled symbols) or in the presence (open symbols) of 30 μM unlabeled Cd. Points shown are means ± SEM evaluated on 3 different cell passages. The lines shown are the best fit curves over the data points (±95% confidence intervals), as obtained according to the first-order rate equation Eq. (1) in the text. The uptake parameters are listed in Table 2.

process since U_0^* is sensitive to unlabeled Cd. The amplitude of this specific uptake component (U_{0s}^* = difference between conditions (1) and (2) in Table 2) appears inversely proportional (mean proportionality factor of 10.2 ± 2.9 for the three cell lines) to the $t_{1/2}$ values of the slow phase of uptake. On the basis of an average cell volume of 3.66 ± 0.20 μl.mg protein^{-1} [7], U_{0s}^* corresponds to an accumulation ratio of intracellular-to-extracellular Cd concentrations varying from a minimum value of 0.3 in PF11 cells to a maximum value of 0.7 in TC7 cells.

Third, there is a stationary phase of Cd uptake (U_e^* parameter in Table 2) which is highly sensitive to cold Cd but almost independent of the cell functional differentiation status under both conditions of incubation. On the basis of the average cell volume reported above, it can be calculated from the U_e^* values that there is a 11.9 ± 1.2-fold or a 1.6 ± 0.3-fold accumulation ratio of intracellular-to-extracellular ^{109}Cd concentrations at equilibrium (α_e) under assay conditions (1) or (2), respectively. For the similar cell densities of 1.2 ± 0.3 mg protein.plate^{-1} measured in 18-day-old monolayers, the U_e^* values estimated in the presence of tracer alone represent intracellular ^{109}Cd contents of 15.6 ± 1.6 pmol.plate^{-1} under uptake conditions where the total Cd content initially present in the uptake media was 300 pmol.plate^{-1}. Clearly, then, Cd depletion from the medium of 5.2 ± 0.5% does not contribute appreciably to the leveling off in Cd accumulation observed in uptake studies such as those shown in Fig. 2.

The results shown in Fig. 2 and Table 2 suggest that cellular functional differentiation status does not greatly affect the general characteristics of Cd uptake in Caco-2 cells. However, since the TC7 monolayers appeared more representative of the adult mature enterocyte (Fig. 1), subsequent experiments were performed exclusively on these cloned cells.

Effect of EDTA in the Stop Solutions on Cd Uptake Measurements

The specific rapid initial phase of 0.3 μM ^{109}Cd uptake (U_{0s}^*), characterized above by its sensitivity to high concentrations of unlabeled $CdCl_2$, could represent external binding to specific membrane sites, in which case it should be possible to reduce it by using a strong Cd chelator such as EDTA in the stop solutions during the washing process. As shown in Fig. 3, washing the Petri dishes with 2 mM EDTA (open circles) significantly lowered Cd uptake values all along the uptake time-course study when compared to the standard washing procedure (filled circles), although the difference between the two treatments was no longer significant at equilibrium (t = 65 min). The net effect is a small increase in the $t_{1/2}$ of equilibration from 16.1 ± 1.7 min in the absence of EDTA to 17.4 ± 2.0 min in its presence. The inset of Fig. 3 shows that Cd uptake can be approximated by straight lines for up to 3-min incubation times under both conditions and clearly demonstrates that, as expected, EDTA in the stop solutions reduced the fast binding component as compared to the control conditions (0.40 ± 0.10 *vs.* 1.14 ± 0.22 pmol.mg protein^{-1}, respectively). The inset of Fig. 3 also indicates that the initial uptake rate is decreased by 25% when EDTA is present during the washing steps (0.42 ± 0.06 *vs.* 0.56 ± 0.05 pmol.min^{-1}.protein^{-1} with and without EDTA, respectively).

Kinetics of Cd Efflux

The results shown in Table 2 demonstrate that ^{109}Cd accumulation at equilibrium initially appears concentrative and is highly sensitive to unlabeled Cd. Accordingly, Cd interactions with intracellular structures may be suspected, as supported by the considerations given in Appendix I. This hypothesis was addressed by looking at the time courses of Cd efflux from TC7 cells preexposed to 0.3 μM ^{109}Cd for 65 min. The results of these

Table 2. Uptake parameter values describing the time course of ^{109}Cd tracer uptake in the different Caco-2 cell lines

	U_0^* (pmol.mg protein^{-1})	U_e^* (pmol.mg protein^{-1})	$t_{1/2}$ (min)	α_e
C#80-90	(1) 0.89 ± 0.21	11.9 ± 0.8	13.1 ± 1.5	10.8 ± 1.3
	(2) 0.30 ± 0.02	1.4 ± 0.2	24.8 ± 3.4	1.3 ± 0.4
TC7	(1) 1.15 ± 0.15	12.7 ± 0.4	17.3 ± 1.3[a]	11.6 ± 0.8
	(2) 0.38 ± 0.07	2.1 ± 0.2	36.2 ± 5.7	1.9 ± 0.5
PF11	(1) 0.81 ± 0.16	14.5 ± 0.9	28.9 ± 3.6[a]	13.2 ± 1.3
	(2) 0.48 ± 0.04	1.6 ± 0.3	42.5 ± 6.4	1.5 ± 0.5

Experimental conditions and analyses were as described in the legend to Fig. 2 showing the uptake time courses in the TC7 and PF11 clones only. (1) and (2) correspond to 0.3 μM ^{109}Cd uptake measured in the absence or presence of 30 μM unlabeled Cd, respectively. The meaning of the uptake parameters U_0^*, U_e^* and $t½$ is given in the text, and the values shown are the best-fit parameters ± SER values corresponding to Eq. (1). The accumulation ratios of intracellular-to-extracellular ^{109}Cd concentrations (α_e) were calculated from the U_e^* values as described in the text. Letter *a* indicates significant differences ($P \leqslant 0.05$) between the two clones TC7 and PF11.

experiments are presented in Fig. 4 where the efflux studies have been conducted in standard Cd-free (filled circles) or EDTA-containing (open circles) media. In both cases, the time course of Cd efflux could be well described by the first-order decay Eq. (3).

As previously noted in Fig. 3, it is also readily apparent in Fig. 4 that the zero-time control efflux (which corresponds to the equilibrium control uptake in Fig. 3) is lower using EDTA-containing than EDTA-free stop solutions (12.3 ± 0.3 *vs.* 14.6 ± 1.4 pmol.mg protein^{-1}). For the 65-min efflux experiment, both the rate ($t_{1/2}$ values of 8.2 ± 3.2 *vs.* 1.5 ± 0.2 min) and extent (values of 12.2 ± 0.3 *vs.* 7.8 ± 0.1 pmol.mg protein^{-1} at 65 min-efflux) of Cd release were greater in the EDTA-containing solution. After correction for the initial binding components in the absence or presence of EDTA (Fig. 3), it can be calculated that up to 55% (7.4 pmol.mg protein^{-1}) of the intracellular Cd initially accumulated (13.5 pmol.mg protein^{-1}) cannot be recovered in the EDTA-containing medium. With an average cell volume of 3.66 μl.mg protein^{-1} [7], this value accounts for a 6.7-fold accumulation of intracellular Cd relative to the Cd concentration initially present in the uptake medium. Note that the amount of Cd recovered in the EDTA-containing medium (7.3 pmol.plate^{-1}) is obviously too small to saturate 2 μmol/ml EDTA [3].

The rapid loss of Cd content in the EDTA-containing solutions undoubtedly contributes to the apparently lower initial rates of Cd uptake recorded when EDTA-containing stop solutions were used (inset of Fig. 3). Accordingly, subsequent experiments were performed using the standard stop solution to minimize efflux during the washing steps.

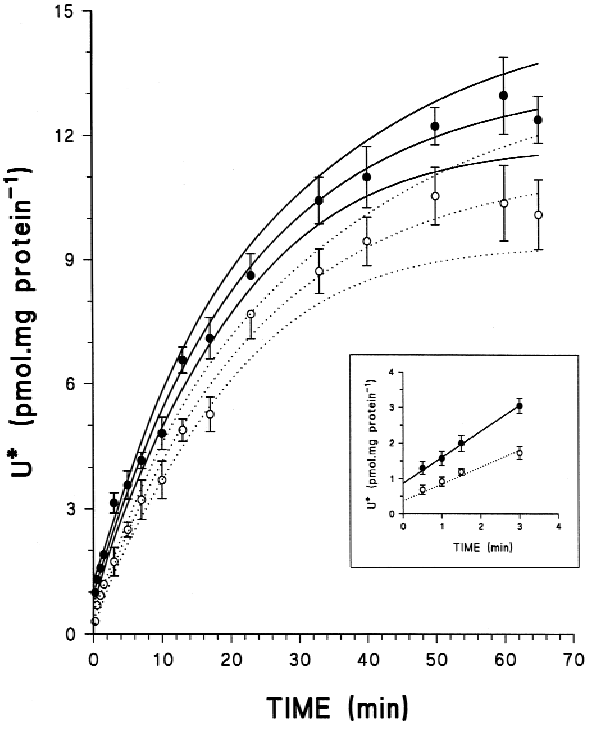

Fig. 3. Effect of EDTA in the stop solutions on Cd uptake measurements. Time course of 0.3 μM ^{109}Cd uptake (*U**) was determined for 18-day-old TC7 cells as described in the text and uptake was stopped with standard cold Cd-free medium (●) or with 2 mM EDTA-containing medium (○). Points shown are means ± SEM evaluated on 3 determinations on the same subculture. Inset: initial short-term Cd accumulation. The lines shown are the best fit curves over the data points (±95% confidence intervals) as obtained according to the first-order rate Eq. (1). (main graph) and to the linear regression analysis (Eq. 2) (inset).

Effects of Ouabain and Sulfhydryl Binding Agents

The experiments described in Fig. 2 and Table 2 demonstrate that unlabeled Cd can compete quite effectively for uptake with ^{109}Cd, which strongly suggests that a transport protein might be responsible for Cd accumulation in Caco-2 cells. Further support for this hypothesis was thus sought by testing the effect of ouabain and

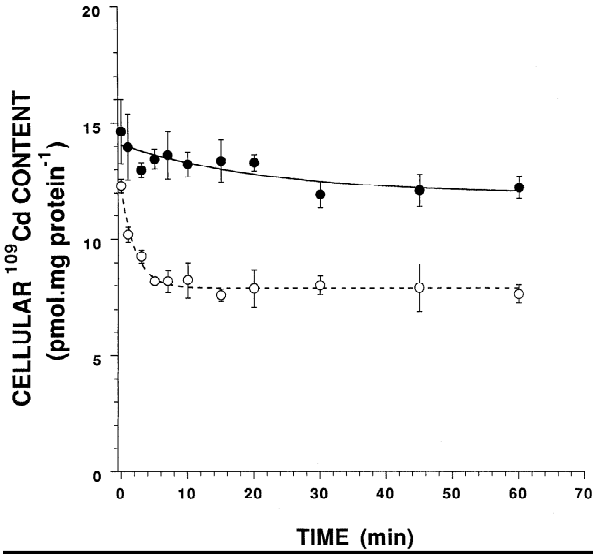

Fig. 4. Kinetics of Cd efflux from 18-day-old TC7 monolayers. The cells were preexposed to 0.3 μM ^{109}Cd for 65 min, and Cd release was determined in standard Cd-free medium (●) or in the presence of 2 mM EDTA (○) for specific times as described in the text. Lines show the best fit curves over the data points (means ± SEM evaluated on 3 determinations on the same subculture) corresponding to the first-order decay Eq. (3).

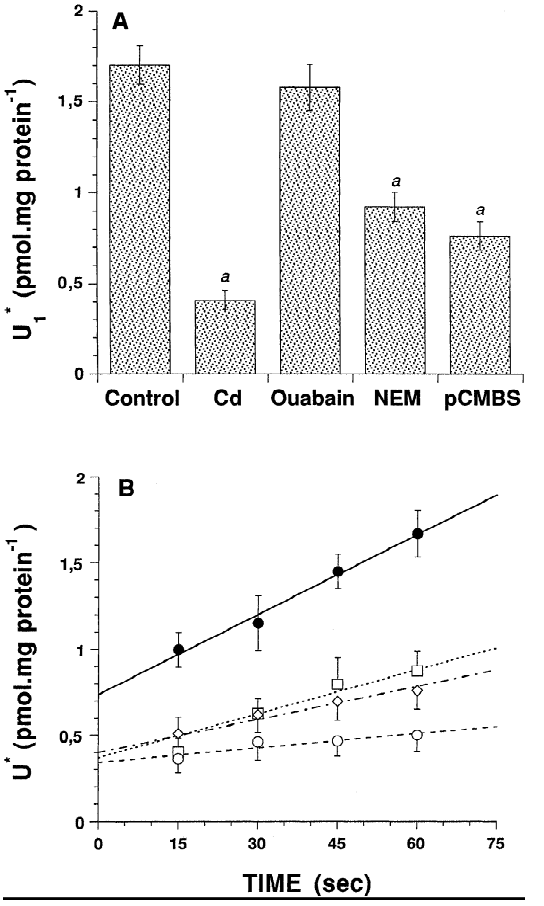

Fig. 5. Effect of ouabain and two SH blockers on the initial uptake of Cd measured at 1 min (U_1^*, *A*) or for different short-term incubations (U*, *B*). 18-day-old TC7 cells were preincubated in the presence of 1 mM ouabain (ouabain), 2 mM NEM (NEM, □) or 2 mM pCMBS (pCMBS, ◇) for 30 min at 37°C and uptake of 0.3 μM ^{109}Cd was determined at room temperature in the presence of the specific inhibitors as described in the text. Uptake experiments were also performed on untreated cells (control, ●) and in the presence of 100 μM unlabeled Cd (Cd, ○). Values shown are means ± SEM evaluated on 5 determinations on the same subculture. The latter *a* indicates significant differences ($P \leq 0.05$) compared with the control value. The uptake parameters obtained following linear regression analyses (Eq. 2) over the data points are listed in Table 3.

SH-reactive agents on Cd uptake. In a first series of experiments, the initial uptakes of 0.3 μM ^{109}Cd (U_1^*) were estimated at 1 min and 20°C following a 30 min preincubation period at 37°C in the presence of the different inhibitors. As shown in Fig. 5*A*, Cd uptake was unaffected by the specific inhibitor of the Na^+-K^+-ATPase pump, but was markedly inhibited following cell pretreatment with 2 mM of either NEM or pCMBS. If ^{109}Cd uptake in the presence of 100 μM unlabeled Cd is taken to represent nonspecific (nondisplaceable) tracer uptake, as seems justified from the results presented in Fig. 2, it can be calculated that NEM and pCMBS inhibit the specific component(s) of Cd uptake (U_{1s}^*) by 60% and 72%, respectively. For both NEM and pCMBS, a preincubation period proved necessary to exert significant inhibition. When NEM and pCMBS were removed from the incubation media prior to uptake measurements, a 40% inhibition level was still observed with the former whereas a non-significant inhibition of only 7% was recorded with the latter (*data not shown*).

To better understand the effect of the SH-reactive agents, experiments similar to those presented in Fig. 5*A* were repeated at a tracer concentration of 0.3 μM ^{109}Cd and uptake was recorded at different time intervals over a 1 min incubation period. The results of these experiments are presented in Fig. 5*B* where it can be appreciated that NEM (open squares) and pCMBS (open diamonds) affected both the initial rate of uptake and the zero-time intercept values (Table 3). Again, if ^{109}Cd uptake in the presence of 100 μM unlabeled Cd is taken to represent nonspecific (nondisplaceable) tracer uptake, it can be calculated from Table 3 that NEM and pCMBS inhibit, respectively, 91 and 84% of the specific U_0^* values (U_{0s}^* in Table 3), 56 and 73% of the specific V_1^* values (V_{1s}^* in Table 3), and 69 and 77% of the specific U_1^* values (U_{1s}^* values can be compiled from the sum of the U_{0s}^* and V_{1s}^* components shown in Table 3).

Kinetic Parameters of Cd Influx

Ideally, because the initial phase of Cd uptake involves both rapid and slow processes (Figs. 2, 3, 5, and Tables 2 and 3), the kinetic parameters of Cd influx should be

Table 3. Effect of NEM and pCMBS on zero-time intercepts (U_0^*) and uptake rates normalized to 1-min uptake (V_1^*)

Conditions	Initial rates (pmol.mg protein^{-1})		Zero-time intercept (pmol.mg protein^{-1})	
	V_1^*	V_{1s}^*	U_0^*	U_{0s}^*
Control	0.91 ± 0.05	0.73 ± 0.09 (100%)	0.76 ± 0.04	0.43 ± 0.07 (100%)
NEM	0.50 ± 0.05	0.32 ± 0.09 (44%)	0.37 ± 0.05	0.04 ± 0.08 (9%)
pCMBS	0.38 ± 0.02	0.20 ± 0.06 (27%)	0.40 ± 0.02	0.07 ± 0.05 (16%)
$CdCl_2$	0.18 ± 0.04		0.33 ± 0.03	

Experimental conditions and analyses were as described in the legend to Fig. 5. Values shown are the best-fit parameters ± SER values obtained by linear regression analyses (Eq. 2) of the data presented in Fig. 5*B*. The uptake parameters U_0^* and V_1^* represent the intercept and slope (normalized to 1 min uptake) of the regression lines, respectively. Specific fractions V_{1s} and U_{0s}^* were calculated by subtraction of the total values obtained in the presence of 100 μM unlabeled Cd from the total values estimated under all other experimental conditions. Percentile values shown in parentheses were calculated relative to the specific values under control conditions arbitrarily taken as 100%.

determined from uptake time-course studies performed at different Cd concentrations (T_o). In principle this approach allows one to estimate the two initial uptake components and to analyze them separately according to Eqs. (5 and 6).

$$V^* = \frac{V_{\max}(T_o)}{K_m + (T_o)} + k_D(T_o) \tag{5}$$

$$U_0^* = \frac{U_{\max 0}(T_o)}{K_{m0} + (T_o)} + K_0(T_o) \tag{6}$$

Eq. (5) assumes that the initial rate of Cd uptake V^* involves: (i) a specific (saturable) process (V_s^*) which obeys Michaelis-Menten kinetics and can be described by the usual kinetic parameters $V_{\max}$ and K_m; and (ii) a nonspecific process such as purely passive diffusion defined by the rate constant k_D. Similarly, Eq. (6) postulates that the rapid initial uptake phase (U_0^*) involves both saturable (U_{0s}^*) and nonspecific processes characterized, respectively, by the kinetic parameters $U_{\max 0}$ and K_{m0}, and the proportionality constant K_0.

Experimentally, however, the low signal-over-noise ratio achieved and the necessarily low number of data points collected in experiments such as those shown in Fig. 5*B* precluded a meaningful separation of the U_0^* and V^* components of the initial uptake at each Cd concentration. Accordingly, the kinetic parameters of Cd influx were evaluated from the initial Cd uptake values measured at a 1 min time point (U_1^*); pure tracer concentrations ranging from 0.1 to 30 μM were used to increase the signal-over-noise ratio of the assays. The data were fitted by nonlinear regression analysis according to Eq. (7).

$$U_1^* = V_1^* + U_0^* \tag{7}$$

in which V_1^* (equivalent to V^* normalized to 1-min uptake) and U_0^* are defined by Eqs. (5) and (6), respectively. This analysis failed to detect the presence of more than one Michaelis-Menten component; Eq. (8)

$$U_1^* = \frac{U_{\max 1}(T_o)}{K_{m1} + (T_o)} + K_{D1}(T_o) \tag{8}$$

was thus found to be sufficient to describe the experimental data fully (curve 1 in Fig. 6*A*) with the following values for the operational kinetic parameters: $U_{\max 1}$ = 17.1 ± 4.8 pmol.mg protein^{-1}; K_{m1} = 3.9 ± 1.2 μM; K_{D1} = 1.65 ± 0.18 pmol.mg protein^{-1}.μM^{-1}.

These values prove satisfactory in two ways: (i) the K_{m1} value predicts 88% and 96% inhibition of U_{1s}^* by 30 and 100 μM unlabeled Cd, respectively, in agreement with the results shown in Table 2 and 3; and (ii) the K_{D1} value predicted by Eq. (9)

$$K_{D1} = k_{D1} + K_0 \tag{9}$$

from the consideration of Eqs. (5–8) is equal to the sum of the individual k_{D1} (0.60 ± 0.13 pmol.mg protein^{-1}.μM^{-1}) and K_0 (1.10 ± 0.10 pmol.mg protein^{-1}.μM^{-1}) values that can be estimated independently, respectively, from the non-specific V_1^* and U_0^* values reported in Table 3 after normalization to 1 μM Cd. Prior correction for the contribution to total uptake of the $K_0(T_o)$ term (curve 2 in Fig. 6*A*), which gives a more realistic view of the Cd uptake process per se, led to identical $V_{\max}$ and K_m values with k_{D1} = 0.55 ± 0.18 pmol.min^{-1}.mg protein^{-1}.μM^{-1}. Similarly, data correction for the previously determined $K_{D1}(T_o)$ term (curve 3 in Fig. 6*A*), which isolates the specific uptake process, led to the $V_{\max}$ and K_m values shown in Fig. 6*B* and resulted in lower SER values associated with the kinetic parameters determination.

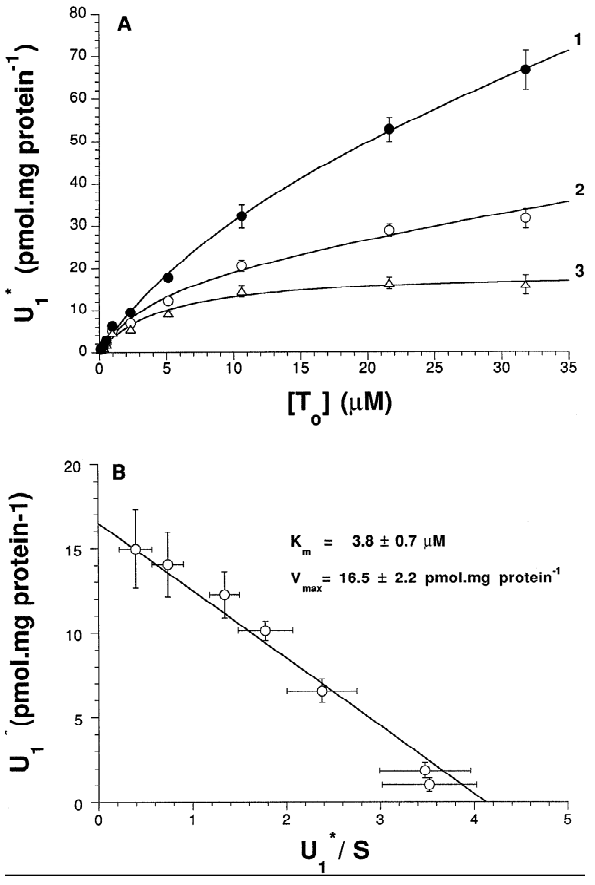

Fig. 6. Determination of kinetic parameters for Cd influx in 18-day-old TC7 cells. Initial Cd uptakes (U_1^*) were estimated by one-time point analysis (1 min) as a function of ^{109}Cd concentrations as described in the text. Data points shown are the means ± SEM evaluated on 5 determinations on the same subculture. (*A*): Direct plot corresponding to measured total uptake (●) or to experimental data corrected for the nonspecific components of 1.10 pmol.mg protein^{-1}.μM^{-1} (○) or 1.7 pmol.mg protein^{-1}.μM^{-1} (Δ) as discussed in the text. The lines shown are the best fit curves over the data points, as obtained by nonlinear regression analysis using Eq. (8). (*B*) Eadie-Hofstee transformation of curve 3 in (*A*) with kinetic parameters as shown.

The Eadie-Hofstee plot shown in Fig. 6*B* and constructed from curve 3 in Fig. 6*A* does not show any sign of upward deviation from linearity. This result is compatible with the hypothesis that the specific and fast initial phase of Cd uptake represents Cd binding on a unique transport protein, in which case the theoretical considerations presented in Appendix II predict that K_{m0} in Eq. (6) should be equal to K_m and K_{m1} in Eqs. (5) and (8), respectively. Further consideration of Eq. (7) would thus lead to equality (10),

$$U_{max1} = V_{max1} + U_{max0} \quad (10)$$

which suggests that the individual contributions of V_{1s}^* and U_{0s}^* to U_{1s}^* measured at any (T_o) should be directly proportional to their maximum values. Since the data reported in Table 3 show that V_{1s}^* and U_{0s}^* measured at 0.3 μM ^{109}Cd account, respectively, for 63% and 37% of the total U_{1s}^* estimated at 1 min, a V_{max1} value of 10.4 pmol.mg protein^{-1} and a U_{max0} value of 6.1 pmol.mg protein^{-1} can be estimated that would be entirely compatible with the available evidence.

Table 4. Zn speciation in the PO_4-free transport medium

Name	% Total
Zn^{2+}	81.2
$ZnCl^+$	8.4
ZnOHCl	2.6
$ZnCO_3$	2.5
$ZnSO_4$	1.8
$ZnHCO_3^-$	1.6

The composition of the transport medium is described in the text. Zn speciation was calculated using the MINEQL$^+$ chemical equilibrium program. Species listed are those representing more than 1% of the total dissolved metal.

Effect of Zinc on Cd Uptake

Since Zn transport has been characterized previously in Caco-2 cells [36] and since Zn and Cd competition for a common transport system has been demonstrated in the pig small intestine [44], various concentrations of Zn ranging from 0.5 to 100 μM were tested as to their ability to alter the initial rates of 0.3 μM ^{109}Cd uptake. However, because MINEQL$^+$ calculations predicted that there was a risk of precipitation reactions under the standard experimental conditions used to this point, these experiments were performed in PO_4-free media. Under these conditions, the relative amounts of the various Zn species representing more than 1% of the total dissolved metal in the uptake medium are listed in Table 4. Note that Zn speciation in both PO_4-containing and PO_4-free media are similar since the majority of the Zn is present as the free Zn^{2+} ion (Table 4), the solubility of which has been increased by PO_4 removal. Similarly, neither the absence of PO_4 nor the presence of Zn can change in a significant way the free Cl^- concentration in the uptake media; it follows that Cd speciation, which is essentially determined by complexation with Cl^- (*see* Table 1), is unaffected by the addition of Zn or the removal of PO_4.

In agreement with these observations, Fig. 7*A* clearly shows that PO_4 removal did not affect the 1-min uptake of 0.3 μM ^{109}Cd (U_1^*) in the absence (Ctrl) or presence (Cd) of 100 μM unlabeled Cd. It can also be appreciated in this figure that Zn concentrations of 5 μM or higher significantly reduced Cd uptake and that the level of inhibition was dose-dependent. The specific U_{1s}^*

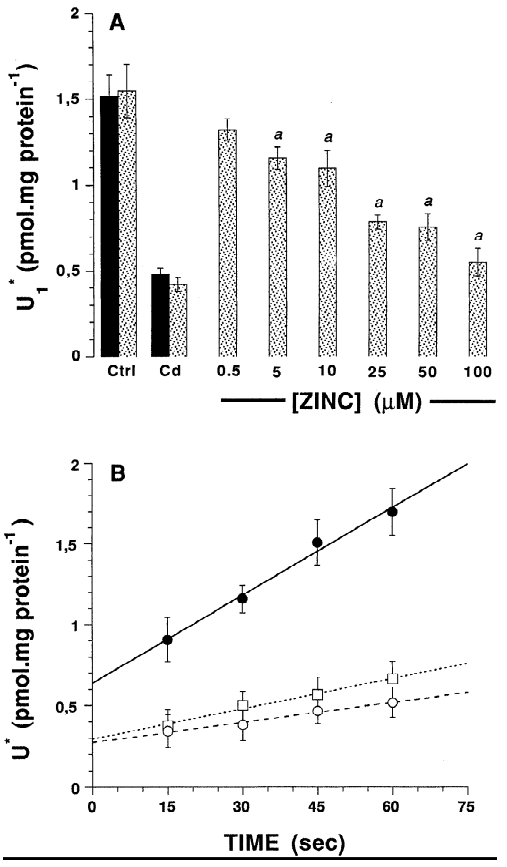

Fig. 7. Effect of Zn on the initial uptake of Cd measured at 1 min (U_1^*) or for different short-term incubations (U^*). (*A*): 18-day-old TC7 cells were exposed in a PO_4-free medium to 0.3 μM ^{109}Cd and different concentrations of Zn ranging from 0.5 to 100 μM. Uptake experiments were also performed using either ^{109}Cd alone (Ctrl) or in the presence of 100 μM unlabeled Cd (Cd) in both the standard (filled columns) and the PO_4-free (dotted columns) media. The letter *a* indicates significant differences ($P \leq 0.05$) compared to control values. (*B*): Cd uptake was measured using ^{109}Cd alone (●) or in the presence of 100 μM Cd (○) or 100 μM Zn (□) in a PO_4-free medium. Linear regression (Eq. 2) analyses over the data points give the following intercept (U_0^*) and slope (V^*) values: $U_0^* = 0.64 \pm 0.08$ (control); 0.28 ± 0.03 (Cd); 0.30 ± 0.03 (Zn) pmol.mg protein^{-1} and $V^* = 1.11 \pm 0.14$ (control); 0.25 ± 0.02 (Cd); 0.36 ± 0.05 (Zn) pmol.sec^{-1}.mg protein^{-1}. In both *A* and *B*, values shown are means ± SEM evaluated on 5 determinations on the same subculture.

fraction of U_1^* was calculated and the resulting data could be fitted successfully to Eq. (11)

$$U_{1s}^* = [U_{1s}^*]_{(\mathrm{Zn})=0} \left(\frac{K_m + (T_o)}{K_m \left[1 + \frac{(Zn)}{K_i} \right] + (T_o)} \right) \qquad (11)$$

which is derived from Eq. (8) by incorporating a competitive mechanism of Zn inhibition with inhibition constant K_i (*data not shown*). The parameters (T_o), K_m and $[U_{1s}^*]_{(\mathrm{Zn})=0}$ in Eq. (11) were fixed to their respective values and a K_i value of 17.3 ± 3.0 μM Zn was estimated by nonlinear regression analysis.

To characterize further the effects of Zn, 0.3 μM ^{109}Cd uptake was also measured at different time intervals over a 1-min incubation period in the presence of 100 μM Zn (Fig. 7*B*). This high Zn concentration (open squares) inhibited both the initial binding component (U_0^*) and the initial rate of tracer uptake (V*), as can be judged from the comparison with tracer uptakes in the presence (open circles) or absence (filled circles) of 100 μM Cd. Because equations similar in form to Eq. (11) would also apply to the V_{1s}^* and U_{0s}^* fractions of V_1^* and U_0^*, it can be predicted that 100 μM Zn should inhibit both components of U_{1s}^* by 84%. In agreement with the competitive inhibition mechanism and the K_i value estimated above, 87% and 94% inhibition of V_s^* and U_{0s}^* could be calculated, respectively, from the slope and intercept values reported in the legend for Fig. 7.

Kinetic Parameters of Cd Accumulation at Equilibrium (U_e^*)

The trapping of Cd by intracellular structures could be responsible for the high accumulation ratios of intracellular-to-extracellular Cd concentrations at equilibrium. As shown by Eq. (A7) in Appendix I, this hypothesis is also compatible with the high sensitivity of U_e^* to unlabeled Cd concentrations (Fig. 2 and Table 2). Therefore, it should be possible to evaluate the contribution of the intracellular process(es) to total uptake by determining the(ir) apparent kinetic parameters at equilibrium. Accordingly, U_e^* was estimated from the 65-min uptake values of 0.3 μM ^{109}Cd measured in cells coincubated with unlabeled Cd concentrations ranging from 0 to 100 μM. This strategy was adopted because the high levels of intracellular ^{109}Cd at equilibrium allowed us to attain high signal-over-noise ratios, as can be appreciated in Fig. 8 from the displacement curve of 0.3 μM ^{109}Cd (T_o) by the increasing concentrations of unlabeled Cd (S_o).

As justified previously [11, 32], nonlinear regression analysis of such data can be performed using a modified Michaelis-Menten equation, which can be obtained by assuming that the unlabeled substrate acts as an ideal competitive inhibitor of the tracer substrate. In the particular case at hand, Eq. (12)

$$U_e^* = \frac{U_{\mathrm{maxe}}\,(T_o)}{K_{me} + (S_o) + (T_o)} + K_{De}\,(T_o) \qquad (12)$$

was used and resulted from the consideration of Eqs. (8) and (11) where: (i) the subscript (*e*) was substituted for (1) in both equations; and (ii) (S_o) was equivalent to (Zn) and $K_i = K_{me}$ in the latter. Eq. (12) predicts that U_{es}^* (defined as the saturable fraction of U_e^*) → 0 when (S_o) → ∞, so that the displacement curve should tend towards a plateau value at full saturation by the unlabeled sub-

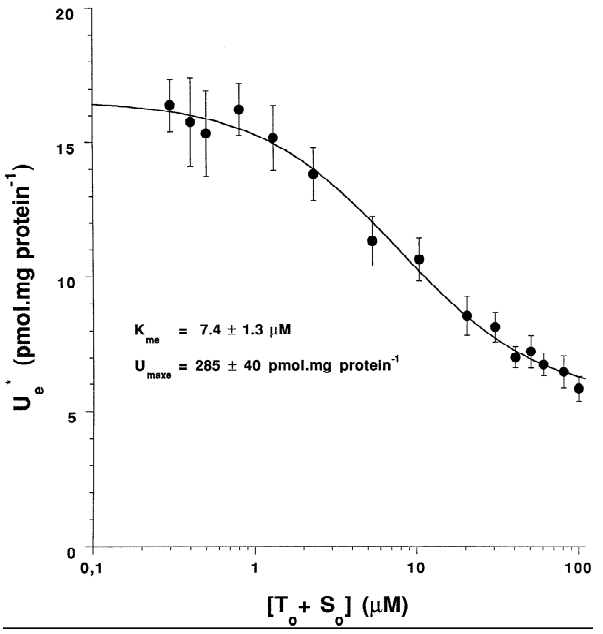

Fig. 8. Kinetic parameters of Cd uptake at equilibrium in 18-day-old TC7 cells. Equilibrium uptake values (U_e^*) were estimated at a 65-min time point as described in the text using a ^{109}Cd tracer concentration (T_o) of 0.3 μM and unlabeled Cd concentrations (S_o) ranging from 0 to 100 μM. Values shown are means ± SEM evaluated on 5 determinations on the same subculture. The line is the best fit curve to Eq. (12) with kinetic parameters values as shown. Note that the log scale on the x axis simply allows a better presentation of the kinetic data [11].

strate. Similarly, over the concentration range where the relation $(S_o) + (T_o) << K_{me}$ applies, Eq. (12) reduces to Eq. (13),

$$U_e^* = \frac{U_{\text{maxe}}}{K_{me}}(T_o) + K_{De}(T_o) \qquad (13)$$

and the displacement curve should also show a plateau in the low range of substrate concentrations.

The experimental data shown in Fig. 8 could be successfully described by a nonlinear regression analysis to Eq. (12) with the following values of the kinetic parameters: K_{me} = 7.4 ± 1.3 μM, U_{maxe} = 285 ± 40 pmol.mg protein^{-1}, and K_{De} = 18.3 ± 1.0 pmol.mg protein^{-1}.μM^{-1}. The nonspecific binding process accounts for 5.5 ± 0.3 pmol.mg protein^{-1} at 0.3 μM ^{109}Cd, thus corresponding to an intracellular concentration of 1.5 ± 0.3 μM or a 5-fold intracellular Cd accumulation over the external medium. The latter value is slightly higher than that shown for TC7 cells in Table 2 at 30 μM external Cd; however, the specific component of equilibrium uptake (11.6 pmol.mg protein^{-1}) can be converted to an intracellular concentration of 3.2 μM for an overall intracellular Cd accumulation of 10.6-fold which compares well to the accumulation ratio α_e of 11.6-fold calculated in Table 2.

Attempts to fit the data in Fig. 8 to model equations assuming 2 specific systems working in the presence or absence of a nonspecific process failed (these models had to be rejected on the basis of either divergence or negative parameter values). Note that the kinetic parameter values reported above and Eq. (13) predict a plateau value of 17.0 pmol.mg protein^{-1} in the low range of substrate concentrations, in agreement with the experimental data shown in Fig. 8.

Discussion

In numerous cell types, including the intestinal mucosa cells, Cd uptake has been shown to be a saturable process relative to increasing Cd concentrations [17, 18, 23]. However, although some data have suggested the involvement of thiol-groups in Cd uptake in rat hepatocytes [18] and red blood cells [17], the question of whether or not Cd entry into cells is mediated by (a) membrane transport protein(s) has been much debated. In this respect, our studies clearly show that Cd accumulation in Caco-2 cells involves a rapid and a slow uptake phase, the latter leading to a complete equilibrium distribution of Cd with $t_{1/2}$ = 17.3 ± 1.3 min in TC7 cells incubated with 0.3 μM radiotracer ^{109}Cd (Fig. 2 and Table 2). Moreover, our results demonstrate that Cd uptake by these cells is a complex phenomenon to which contribute both specific and nonspecific transport and binding processes.

Fast and Slow Initial Phases of Cd Uptake

The first and rapid initial step of Cd uptake clearly shows up as a nonzero intercept on the y-axis in our uptake time-course studies (Figs. 2, 3, 5*B* and 7*B*). Parts of this fast initial phase (U_0^*) involves a specific component (U_{0s}^*) which is abolished by 100 μM of either Zn (Fig. 7*B*) or unlabelled Cd (Figs. 5*B* and 7*B*), by SH-reactive agents (Fig. 5*B*), and by 2 mM EDTA present in the stop solutions (Fig. 3). Conversely, that part of U_0^* that survives all of these treatments should be considered as nonspecific and can be tentatively attributed to represent the dead space in our experiments (unwashed tracer, binding to nonspecific membrane sites, etc.).

In the most general case where a transported molecule becomes subject to intracellular reactions, as would occur for Cd binding to intracellular structures following transport, one may expect to find rather complex patterns of initial uptake. For example, a model of transport followed by metabolism [50] predict the existence of burst-(downward deviations) and/or lag-(upward deviations) type kinetics during the approach to steady state. The first case would mostly occur under conditions where transport is slightly faster than intracellular reactions and

the second in the reverse situation. In the limit case where transport is very fast, the burst kinetics might become too rapid to be observed over the time scale of the analysis. However, if the amplitude of the burst phase is significant, it may show up as a nonzero intercept on the y-axis of the uptake time curves, such as it appears clearly in our studies (Figs. 2, 3, 5*B*, 7*B*). This hypothesis was thus evaluated as to its compatibility with our experimental data using the so-called fast-transport slow-intracellular binding model (*see* Appendix I, 1), and it was ruled out on the basis that it cannot explain the saturation kinetics observed in Fig. 6. We therefore conclude that the time courses of Cd uptake represent, at least in part, the kinetics of Cd transport.

The involvement of (a) specific membrane transport protein(s) during the slow phase of Cd uptake is supported by the following pieces of evidence: (i) the initial rate of tracer uptake (V^*) is highly sensitive to an excess of unlabeled Cd (Figs. 2, 5*B*, and 7*B*), and saturation of initial Cd uptakes (U_1^*) with increasing ^{109}Cd concentrations could be successfully demonstrated (Fig. 6); (ii) V^* is sensitive to SH-reactive agents including pCMBS, which is impermeant to plasma membranes (Fig. 5*B*); (iii) U_1^* is inhibited by Zn (Fig. 7*A*) for which a saturable transport process has been demonstrated previously in Caco-2 cells [36], and the K_i value of 17.3 ± 3.0 μM estimated at 20°C for competitive Zn inhibition of Cd uptake is compatible with the K_m value of 41 μM previously determined at 37°C for Zn transport in this cell line [36]; and (iv) Cd uptake in Caco-2 cells is at least partially reversible and Cd release is very fast in the presence of EDTA, which acts as a diffusional sink for Cd efflux when present in the efflux medium (Fig. 4). Conversely, that part of V^* that proves insensitive to 100 μM of either Zn (Fig. 7*B*) or unlabeled Cd (Figs. 5*B* and 7*B*) and to SH-reactive agents (Fig. 5*B*) should be considered as nonspecific; this component of Cd uptake can be attributed to simple passive diffusion through the cell membrane in our experiments. In agreement with this view, a purely diffusive transport process with an apparent k_{D1} value of 0.55 ± 0.18 pmol.min^{-1}.mg protein^{-1}.μM^{-1} could be demonstrated during the kinetic analyses (Fig. 6).

Cd Uptake Mechanism(s) Involved During the Initial Phase

The specific fractions of U_0^* (U_{0s}^*) and V^* (V_s^*) characterizing, respectively, the rapid and slow phases of initial Cd uptake (U_{1s}^*), appear similarly sensitive to 100 μM of either Zn (Fig. 7*B*) or unlabelled Cd (Figs. 5*B* and 7*B*) and to SH-reactive agents (Fig. 5*B*). Moreover, the kinetic studies relative to Cd (Fig. 6) and Zn (Fig. 7*A*) concentrations, which were performed at a 1-min time point, analyzed both phases simultaneously. The question arises, then, from the absence of heterogeneity noted in Fig. 6, as to whether U_{0s}^* could represent binding to a unique transport protein and, as such, be part of the transport mechanism itself. The latter hypothesis is indeed compatible with the theoretical considerations given in Appendix II, which predict in this case that both the binding and transport phases of uptake would show similar K_m values (3.8 ± 0.7 μM, Fig. 6). Although necessary to support our hypothesis, the theoretical considerations alone may not be sufficient to exclude the possibility that the two uptake phases could as well belong to different entities such as an ion channel and a carrier protein working in parallel. However, this possibility appears unlikely since the demonstration that U_{0s}^* is sensitive to EDTA present in the stop solutions (Fig. 3) strongly suggests that this component represents external binding to specific membrane sites rather than fast Cd entry and equilibration across the cell membrane.

The hypothesis that the rapid phase of Cd uptake might represent fast Cd binding to a unique transport protein is further supported by the observation that U_{0s}^* is higher in the TC7 and C#80–90 cells as compared to the PF11 clone and appears inversely proportional to the $t_{1/2}$ of the slow phase estimated in the respective cell lines. If this assumption is correct, the theoretical considerations given in Appendix II suggest that it should be possible to estimate an upper limit value of the turnover number of the transport protein from the V_{max}/U_{max0} ratio; a value of 1.7 min^{-1} can be calculated from the kinetic parameters determined in the Results. This value appears quite low when compared, for example, to the turnover number of 5–125 sec^{-1} (300–7500 min^{-1}) usually reported in the literature for the Na/glucose cotransporter, a typical carrier-mediated process in the intestinal brush-border membranes [29]. Notwithstanding the fact that U_{max0} might represent high affinity Cd binding to membrane proteins unrelated to Cd transport, such a huge difference is compatible with the similarly big difference that can be noted between the V_{max} values (expressed in pmol.min^{-1}.mg^{-1} protein) of Cd (10.4 in the present studies) and α-methylglucose (440 in [7]) transport in Caco-2 cells. Cadmium uptake in these cells thus occurs through a relatively low capacity process when compared to a carrier-type mechanism like sugar transport.

While the existence in Caco-2 cells of a unique, carrierlike mechanism for Cd transport appears supported by the results discussed so far, the nature of the transport protein involved cannot be readily assessed from our studies. From the absence of any significant effect on the initial uptake following cell pretreatment with ouabain (Fig. 5*A*), it can be inferred that the transport mechanism is unlikely to be secondary active because the inhibition of the Na pump would have led to the collapse of most of the ion gradients at the time of the

transport measurements. It can also be rationalized that the transport mechanism is unlikely to occur through a primary active Ca(Cd)-pump, which should have acted as an extrusion mechanism in the presence of intracellular ATP. A similar consideration also holds for the Na/Ca(Cd) and Ca/Ca(Cd) exchange activities in the presence of Na and Ca gradients, as was the case in our experiments. Note too that all of our experiments were performed in the presence of 2.5 mM Ca to minimize any cellular Ca release and to maintain well-formed tight junctions and intact monolayers. Under these conditions, rapid Cd uptake at a concentration close to four orders of magnitude lower than Ca could be demonstrated. Increasing the Ca concentration to 25 mM did not significantly affect the initial uptake rate (*data not shown*). It seems very unlikely, then, that Cd uptake in Caco-2 cells, as measured in our studies, occurs through a Ca transport route since Ca in the latter experiments was in excess relative to both the Cd concentration (0.3 μM) and to the K_m value for Ca of around 1 mM previously determined for intestinal epithelial cells [47].

Slow-transport, Fast-intracellular Binding Mechanism of Cd Uptake

Once the slow phase of Cd uptake has been completed, there is a 11- to 13-fold accumulation ratio of intracellular-to-extracellular ^{109}Cd concentrations (α_e) that does not seem related to the cell differentiation status (Table 2). In contrast, the half-times ($t_{1/2}$) of ^{109}Cd equilibration appear to be longer in the PF11 clone than in the more differentiated TC7 cells, and they are also increased upon addition of unlabeled Cd in the uptake medium (Table 2). Similarly, ^{109}Cd uptake at equilibrium is highly sensitive to unlabeled Cd and lower α_e values are observed in the presence of 30 μM Cd (Fig. 2). Taken together, these results indicate that intracellular binding rather than active transport is a major determinant of the kinetics of Cd uptake. Indeed, if one assumes a general model of transport followed by intracellular binding, the $t_{1/2}$ values would reflect the kinetics of Cd equilibration through both the transport and intracellular binding steps. Unlabeled Cd would compete with ^{109}Cd through both reactions, so that, in agreement with our results, higher $t_{1/2}$ and lower plateau values would be observed.

The efflux experiments suggest that Cd is both tightly and loosely bound to intracellular proteins (or organelles), the loosely-bound fraction accounting for 45% of intracellular Cd and for a 5.5-fold accumulation ratio (Fig. 4). Although the presence of more than one binding component might be anticipated from these considerations, our kinetic data at equilibrium were found compatible with a model equation that assumes a single class of specific intracellular binding sites only, with values of 7.4 ± 1.3 μM and 285 ± 40 pmol.mg protein^{-1} for the parameters K_{me} and $U_{\max e}$, respectively (Fig. 8). This result is compatible with the existence of different classes of binding sites showing similar affinities and/or with the possibility that the contribution to total binding of ligands with either higher or lower affinities would be undetectable in our analysis. In this respect, low affinity ligands could well account for (at least part of) the nonspecific binding fraction of 5.5 ± 0.3 pmol.mg protein^{-1} which was revealed in our data for 0.3 μM ^{109}Cd at equilibrium (Fig. 8), as would be compatible with the predictions of Eq. (12) when $(S_o) + (T_o) \ll K_{me}$. In this context, the meaning of the K_{me} and $U_{\max e}$ values given above may appear questionable. Their significance was evaluated further in Appendix I,2 where it is concluded that both parameters can be considered as valid operational parameters to address the following issue.

In the context of the proposed model of Cd uptake followed by intracellular binding, the question of the meaning of the kinetic parameters $V_{\max}$ and K_m estimated during the initial phase of uptake is tightly linked to the corollary of which of the transport or binding reactions represents the rate-limiting step during Cd uptake. To answer the latter question is quite easy in general, once the kinetic parameters of influx and binding are known; as shown in Appendix I,3, transport is the rate-limiting step of Cd uptake at all Cd concentrations. Accordingly, the kinetic parameters determined in our studies under initial uptake conditions do represent the kinetic parameters of the transport protein. Note that the slow-transport fast-intracellular binding model of Cd uptake also predicts close-to-zero concentrations of unbound intracellular ^{109}Cd during influx due to the high buffering capacity of intracellular binding. This may in turn explain why the steady-state accumulation ratio of intracellular-to-extracellular Cd concentrations (α_{ss} in Appendix I,1) is relatively insensitive to the membrane potential (and, hence, to the presence of ouabain) during the initial phase of uptake.

Caco-2 Cell Line as a Valuable *In Vitro* Model

Although cell differentiation status did not greatly affect intracellular Cd accumulation at equilibrium (Table 2), Cd uptake occurred more slowly in the PF11 than in the TC7 cells (Fig. 2). This difference could reflect a lower expression of the transport protein itself in the former cells and may indicate that the transport protein is found preferentially associated with mature enterocytes. This assumption appears compatible with recent studies showing that the expression of the Na^+-D-glucose cotransporter (SGLT-1) is also lower in PF11 as compared to TC7 cells [31], but does not readily explain why similar time courses of Cd uptake were observed in TC7 clones and in the less-differentiated parent cell line C#80–90 (Table 2). Alternatively, then, since the com-

mon lineage of the different cell lines used in our studies would argue against the possibility that they express different transport systems, it can be proposed that Cd transport expression in Caco-2 cells is also regulated by a mechanism that has yet to be discovered but might involve intracellular molecules responsible for internal Cd trapping such as metallothionein, which was shown to decrease Cd efflux from the intestine [34], or a cysteine-rich protein recently isolated from the rat intestine [28]. Further studies will be needed to determine the putative role of such proteins in the regulation of Cd uptake and trapping in the small intestine.

To our knowledge, this is the first study to evaluate the kinetic parameters of Cd transport into enterocytelike cells. Previous studies in the rat jejunum using the *in vitro* perfusion [14] or everted gut sac [23] techniques also postulated the existence of a specific Cd transport mechanism with K_m values of 0.1–0.2 mM or 27.9 ± 11.6 μM and V_{max} values of 10 or 0.8 ± 0.3 nmol. $min^{-1}.g^{-1}$ tissue, respectively. Given the heterogeneity of intestinal tissue, the presence of unstirred water layers that may affect the determination of the kinetic parameters of transport using the latter two techniques [5], and the differences in transport assay conditions, it is difficult to make meaningful comparisons between these studies in the rat intestine and ours in Caco-2 cells, but for the fact that they all show that Cd uptake involves a rather high affinity transport process. Also, none of these studies discriminate among the various Cd species present in the transport medium. More than one of the Cd species listed in Table 1 may conceivably participate in the transport process, though our kinetic data did not reveal any heterogeneity. Accordingly, the K_m values reported at this time should be considered as operational parameters only. Finally, none of these studies have addressed the question of the polarization of the transport process. Caco-2 cells can be successfully grown on filters [21], and studies are now in progress in our laboratory to answer this question using this promising cell culture model.

This research was supported by a grant from the Canadian Network of Toxicology Centers (CNTC). The authors thank Dr. Alain Zweibaum who kindly supplied us with the clones TC7 and PF11, as well as Julie Poirier and Michelle Geoffroy-Bordeleau for technical assistance.

Appendix I

Kinetics of Cd Uptake in the Presence of Intracellular Binding Structures

In the following, it is assumed that intracellular Cd binding occurs on a unique class of specific sites. This hypothesis is made for simplicity only and does not restrict in any way the conclusions to be drawn in this appendix because of the additivity principle should there be more than one class of specific site involved in the binding process. The notations (T_o) (^{109}Cd concentration in the incubation medium), (T_i) (unbound ^{109}Cd concentration in the intracellular compartment, (P_i) (free intracellular concentration of a putative protein of total concentration P_T involved in the binding process), and (PT_i) (intracellular concentration of protein-bound ^{109}Cd) are used consistently throughout the text. Moreover, the (P_i) and (PT_i) terms are linked through the conservation Eq. (A1).

$$P_T = (P_i) + (PT_i) \tag{A1}$$

(*1*) *Testing the Validity of the Fast-Transport Slow-intracellular Binding Model*

The fast-transport slow-intracellular binding model assumes that the rate of Cd transport is very fast as compared to the rate of Cd binding, so that a stable distribution ratio of intracellular-to-extracellular ^{109}Cd concentrations ($\alpha_{ss} = (T_i)/(T_o)$) has been reached at the time of initial uptake measurements. Since the conclusions to be drawn below rely heavily on this hypothesis, its validity may need to be assessed first.

From its definition, α_{ss} is equivalent to an equilibrium constant that should assume a value of 1 according to the hypothesis above, provided that the molecule: (i) is neutral and is transported through a channel- or simple carrier-type of mechanism, and (ii) is not involved in any fast reaction once transported into the cells. As shown in Table 1, however, Cd speciation is dictated by the Cl^- ion concentration in the incubation medium and both a $CdCl^+$ complex and the Cd^{2+} ion coexist in solution. Since there is a ≈10-fold gradient of intracellular-to-extracellular Cl^- concentrations across the membrane of most living cells, intracellular Cd speciation will be affected and one would expect increased concentrations of the above two species relative to both $CdCl_2$ or $CdCl_3^-$ complexes. Indeed, for such positively charged entities, one would predict a major effect of the membrane potential on the distribution ratio with $\alpha_{ss} > 1$ at negative potentials such as occur across the boundary of most living cells. Internal Cd concentrations might also be affected by the existence of extrusion mechanisms which, were they acting alone, would give $\alpha_{ss} < 1$. Among these, one may have to consider the putative Na/Ca(Cd) and Ca/Ca(Cd) exchange activities under the Na and Ca gradient conditions prevailing under our experimental conditions, as well as the Ca(Cd)-ATPase in the presence of intracellular ATP. Clearly, then, α_{ss} is equivalent to an equilibrium constant in the thermodynamic sense only because its value is dictated by the magnitude of the different ion gradients and by the cell polarization status at the time of uptake measurements. Conversely, any factor associated with an increased rate of Cd uptake (as achieved, for example, upon increasing the substrate concentration in the uptake medium) that would affect the thermodynamic driving forces acting on the system would in turn affect the relative value of α_{ss}. The demonstration in Fig. 5*A* that the ouabain-induced inhibition of Na,K-ATPase activity, the main determinant of the resting membrane potential and ion gradients to be found in living cells, does not affect initial Cd uptakes significantly, is strong evidence suggesting that none of the mechanisms discussed above are in fact, either alone or in combination, crucial parameters affecting the α_{ss} value. The argument is indeed strengthened by the previous demonstration that ouabain was an effective inhibitor of α-methylglucose transport through the Na/glucose cotransporter in Caco-2 cells [7]. In the following discussion, then, α_{ss} will be considered as a true constant of unknown value. Note that the question of the nature of the transport mechanism involved in Cd uptake is irrelevant to the following considerations.

According to the above hypotheses, intracellular binding can be described by Scheme 1 depicted in Fig. A1, in which T_i binds in an irreversible way to P_i during the initial steady-state phase of uptake with a microscopic rate constant k_{on} to form the complex PT_i. There-

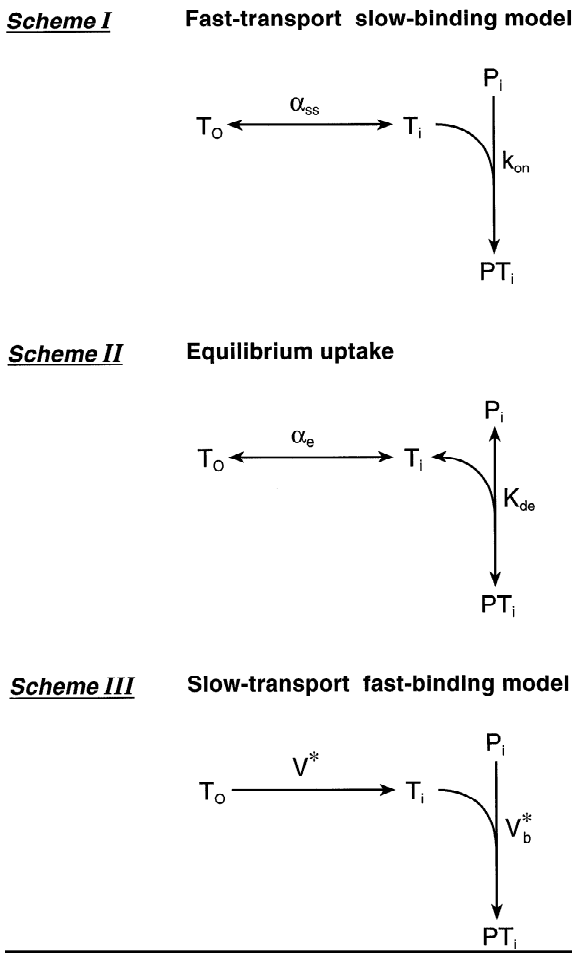

Fig. A1. The different models of Cd transport and intracellular binding considered in Appendix I. In scheme I, it is assumed that transport is very fast, so that intracellular ^{109}Cd (T_i) has equilibrated with outside ^{109}Cd (T_o) before any significant binding can occur onto an intracellular protein (P_i) to give the bound complex PT_i. $\alpha_{ss} = (T_i)/(T_o)$ represents the steady-state distribution of ^{109}Cd during the initial phase of uptake, while k_{on} is the microscopic rate constant of the binding process. In scheme II, it is assumed that the system has proceeded toward full equilibrium. $\alpha_e = (T_i)/(T_o)$ represents the equilibrium distribution of ^{109}Cd while K_{de} is the intrinsic affinity constant of the intracellular binding reaction. In scheme III, it is assumed that the rate of transport (V^*) is very slow as compared to the rate of intracellular binding V_b^*. The situation depicted applies to the steady-state phase of initial uptake. More details are given in the text.

fore, the initial rate (V^*) of Cd binding, which would in this model account for the initial rates of Cd uptake in our studies, is given by Eq. (A2).

$$V^* = \frac{d(PT_i)}{dt} = k_{on}\,(P_i)\,(T_i) \tag{A2}$$

Noting that $(P_i) \approx P_T$ under initial rate conditions because of Eq. (A1), and that $(T_i) = \alpha_{ss}\,(T_o)$ according to the definition of α_{ss} given above, Eq. (A2) can be transformed to Eq. (A3).

$$V^* = k_{on}\,P_T\,\alpha_{ss}\,(T_o) \tag{A3}$$

Integration over short time ranges (over which the steady-state assumption holds) thus leads to Eq. (A4)

$$U_s^* = [k_{on}\,P_T\,\alpha_{ss}\,(T_o)]\cdot t + \alpha_{ss}\,(T_o) \tag{A4}$$

which should describe the time course of specific Cd uptake (U_s^*) during the initial phase and can be used to predict the extent of initial Cd uptake measured at a 1-min time point (U_1^*) as given by Eq. (A5).

$$U_{1s}^* = V_{1s}^* + U_{0s}^* \tag{A5}$$

The latter equation is equivalent to Eq. (7) in the main text when the specific fractions of uptake are the only ones considered. Note that the second term in Eq. (A4) accounts for the fact that (T_i) is also measured in the uptake experiments.

The fast-transport slow-intracellular binding model predicts that initial uptakes should increase linearly with increasing tracer concentrations, in contrast with the data shown in Fig. 6. Note that this model also predicts the absence of unlabeled substrate concentration effects on the rapid initial uptake phase (the zero-time intercept that would be fixed by the distribution ratio α_{ss}). It must be concluded, then, that the saturation observed in these studies represents, at least in part, the kinetics of Cd transport through a saturable process.

(*2*) *Equilibrium Uptake*

At equilibrium Cd uptake, there is no net flux through the transport and binding steps, so that the situation can be described by Scheme II in Fig. A1 in which α_e is the distribution ratio of intracellular-to-extracellular ^{109}Cd concentrations ($\alpha_e = (T_i)/(T_o)$ at equilibrium) and K_{de} represents the dissociation constant of the binding reaction according to Eq. (A6)

$$K_{de} = \frac{(P_i)\,(T_i)}{(PT_i)} \tag{A6}$$

The kinetics of Cd binding at equilibrium where $(PT_i) = U_{es}^*$ would thus be described by Eq. (A7)

$$U_{es}^* = \frac{P_T\,(T_i)}{K_{de} + (T_i)} \tag{A7}$$

which can be easily obtained from the combination of Eqs. (A1) and (A6). Introducing the distribution ratio α_e into Eq. (A7) thus leads to Eq. (A8)

$$U_{es}^* = \frac{P_T\,\alpha_e\,(T_o)}{K_{de} + \alpha_e\,(T_o)} \tag{A8}$$

and, then, to Eq. (A9) after division of the numerator and denominator terms by α_e

$$U_{es}^* = \frac{P_T\,(T_o)}{K_{me} + (T_o)} \qquad \text{with} \qquad K_{me} = \frac{K_{de}}{\alpha_e} \tag{A9}$$

Eq. (A9) is similar in form to Eq. (12) in the main text after proper handling as described there and noting that $U_{\max e} = P_T$.

As discussed in the first section of Appendix I for α_{ss}, the distribution ratio α_e is equivalent to a thermodynamic equilibrium constant, the value of which will be fixed by the driving forces acting on the system at equilibrium and is independent of the nature of the different transport systems involved in Cd transport. Note that α_e should

have a higher value than α_{ss} because the buffering capacity of the intracellular structures leading to $(T_i) \approx 0$ under the initial phase of uptake (*see below*) would have been exhausted at equilibrium. In principle, a precise value of α_e could be determined by measuring (T_i) at equilibrium. However, such measurements can hardly be made using noninvasive techniques and the use of invasive techniques would prove inappropriate for this purpose. If one assumes, however, that the main driving forces at equilibrium are not much affected on increasing Cd concentrations, as seemed justified in the case of α_{ss}, the α_e value can be estimated from our studies under the experimental conditions where intracellular binding was nearly saturated by unlabeled Cd. Accordingly, the α_e value should be close to 1 from the data shown in Table 2.

For simplicity, we have assumed $\alpha_e = 1$ in section 3 below. Note, however, that our calculations according to this assumption may be conservative because the U_{maxe}/K_{me} ratio increases for increasing values of α_e. Note also that the U_{maxe} value of 285 ± 40 pmol.mg protein^{-1} (Fig. 8) would represent the total number of intracellular binding sites and that this conclusion is valid whether the value is determined from either the (T_i) or the (T_o) values.

(3) *Testing the Validity of the Slow-transport Fast-intracellular Binding Model*

The slow-transport fast-intracellular binding model assumes that the rate of Cd transport (V_t^*) is very low as compared to the rate of Cd binding (V_b^*), so that (T_i) entering the cells binds immediately to the intracellular structures following a unidirectional reaction. Accordingly, during the steady-state phase of initial Cd uptake where equation (A10) holds,

$$\frac{dT_i}{dt} = V_t^* - V_b^* = 0 \tag{A10}$$

The (T_i) value assumes a close-to-zero value and the transport step can be considered as unidirectional. Thus V_t^* (the net transport rate) $= V^*$ (the initial rate of transport) and Cd accumulation into cells measured as V_b^* measures the kinetics of transport. The situation is depicted in Scheme III of Fig. A1.

To evaluate the validity of this hypothesis is quite easy once the kinetic parameter values of transport and binding are known. Firstly, the relative rates of transport and binding can be estimated relative to a similarly low $(T_o) = (T_i)$ value << both K_m and K_{me}. Under these conditions, Eq. (5) in the main text (relative to the specific term only) for V^*, and Eq. (A9) above can be rewritten as shown in Eq. (A11)

$$V^* = \frac{V_{max}}{K_m}(T_o) \qquad \text{and} \qquad V_b^* = \frac{P_T}{K_{me}}(T_o) \tag{A11}$$

Similarly, the relative rates of transport and binding can be estimated relative to saturating concentrations of (T_o) and (T_i), in which case both K_m and $K_{me} \ll (T_o)$ and (T_i) and Eq. (A12) would apply.

$$V^* = V_{max} \qquad \text{and} \qquad V_b^* = P_T \tag{A12}$$

The V_b^*/V^* ratios calculated from Eqs. (A11–12) and the kinetic parameter values given in the text show that the binding rate exceeds the transport rate by a factor of 14-fold at very low substrate concentration and by a factor of 27-fold under saturating substrate conditions. Accordingly, it can be concluded that Cd transport is the rate-limiting step of Cd uptake at all substrate concentrations, and that the kinetic parameters determined in our studies under initial rate conditions do represent the kinetic parameters of the transport protein. Note that the above figures are conservative because the B_{maxe} value of 285 ± 40 pmol.mg protein^{-1} used in the calculations may only represent a lower estimate of the total number of binding sites (Figs. 4 and 8).

Appendix II

Testing the Hypothesis that the Specific Initial Step of Cd Uptake Might Represent Fast Cd Binding to a Unique Transport Protein

The experiments shown in Fig. 6 estimated Cd uptake at a 1-min time point (U_1^*), so that the contributions to total uptake of both the rapid (U_0^*) and slow (V_1^*) phases of initial Cd uptake are in fact included in the measurements, as shown by Eq. (7) in the main text. In the most general case, then, one would expect to detect some kinetic heterogeneity during the analysis of U_1^* relative to Cd concentrations unless the kinetic parameter values characterizing the specific V_{1s}^* (V_{max} and K_m) and U_{0s}^* (U_{max0} and K_{m0}) terms in Eqs. (5 and 6) given in the main text fortuitously preclude the kinetic separation of the two elements of U_{1s}^*. However, in the particular case where the V_{1s}^* and U_{0s}^* fractions of U_{1s}^* could be attributed to the same protein, it will be shown that the calculations involved in the determination of the algebraic expressions characterizing V_{1s}^* and U_{0s}^* lead inevitably to the conclusion that the relationship $K_{m0} = K_m$ should hold.

The formal demonstration of the latter point is rather tedious given that an *n*-states transport protein (*N*) that may involve a number of intermediate complexes to which *T* is bound (and, thus, may contribute to the measured U_{0s}^* fraction of uptake), not all of which, however, may lead to (a) substrate releasing step(s) (and, thus, contribute to the V_{1s}^* fraction of uptake). For simplicity, then, we choose the mobile carrier model of membrane transport, a version of which (the iso uni uni system) has been thoroughly analyzed by Segel [39], to demonstrate the general principle validating this conclusion.

The simple carrier model considered here is shown in Fig. B1*A*. The carrier binding sites are alternatively oriented toward the inside (N_1) or the outside (N_2) of the membrane surface, and outside ^{109}Cd (T_o) binding leads to the intermediate binary complex N_3 from which *T* is released in the intracellular compartment (T_i). To make the calculations as simple as possible, it is assumed in Fig. B1A that: (i) the substrate releasing step is unidirectional as justified under initial rate conditions, and (ii) there is only one intermediate complex, as justified by the fact that steady-state kinetics do not allow one to distinguish all of the intermediate complexes involved in isomerization reactions that are not directly linked to the substrate binding steps [39].

According to these hypotheses, the distribution of the different carrier species at the steady state is linked through the conservation Eq. (B1),

$$N_T = N_1 + N_2 + N_3 \tag{B1}$$

so that each of the different carrier forms can be expressed relative to N_T (total carrier concentration) using the three King-Altman interconversion patterns applying to this model and shown in Fig. B1*B*. The carrier state distribution thus conforms to Eqs. (B2–4)

$$\frac{N_1}{N_T} = \frac{k_{21}\,k_{32} + k_{21}\,k_{31} + k_{23}\,k_{31}\,(T_o)}{D} \tag{B2}$$

$$\frac{N_2}{N_T} = \frac{k_{12}\,k_{32} + k_{12}\,k_{31}}{D} \tag{B3}$$

$$\frac{N_3}{N_T} = \frac{k_{12}\,k_{23}\,(T_o)}{D} \tag{B4}$$

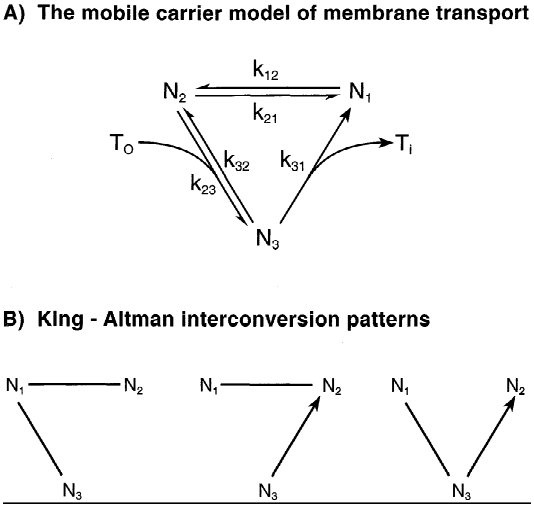

Fig. B1. The mobile carrier model of membrane transport considered in Appendix II. In (*A*), the model is depicted under the initial steady-state phase of transport. Outside ^{109}Cd (T_o) binds to the outwardly oriented substrate site on the free carrier (N_2) to give the transporter-substrate complex N_3 from which ^{109}Cd is released intracellularly (T_i) to generate the inward configuration of the transporter (N_1). The N_1 to N_2 transition represents the free carrier recycling step. The k_{ij} terms represent the microscopic rate constants of the different reactions involved. In (*B*), the King-Altman interconversion patterns applying to the model shown in (*A*) are depicted. These were used to obtain Eqs. (A2–4) given in the text.

in which D is the sum of all numerator terms in Eqs. (B2–4) and can thus be expressed as shown in Eq. (B5)

$$D = (k_{12} + k_{21})(k_{31} + k_{32}) + k_{23}(k_{12} + k_{31})(T_o) \tag{B5}$$

The initial rate of tracer uptake (V_s^*) is given by Eq. (B6)

$$V_s^* = k_{31} N_3 \tag{B6}$$

while the fraction of (T_o) bound onto the carrier (U_{0s}^*) is given by Eq. (B4). The algebraic expressions of the different kinetic parameters thus follow from these considerations and are listed in Eqs. (B7–9).

$$V_{max} = k_{cat} N_T = \frac{k_{12} k_{31} N_T}{k_{12} + k_{31}} \tag{B7}$$

$$U_{max0} = \frac{k_{12} N_T}{k_{12} + k_{31}} \tag{B8}$$

$$K_m = K_{m0} = \frac{(k_{12} + k_{21})(k_{31} + k_{32})}{k_{23}(k_{12} + k_{31})} \tag{B9}$$

The latter equation is compatible with the absence of kinetic heterogeneity noted during the analysis of the data shown in Fig. 6 and would represent a necessary condition to validate the hypothesis that transport and initial binding are part of the same transport mechanism (it may not be sufficient to prove the point, however, because of the limits imposed on the kinetic separation of heterogeneous systems). The general principle underlying the calculations above leads to the prediction that the denominator expressions for those carrier species involved in transport and binding should always be the same, independently of the model being considered and of the specific hypotheses under which the characteristic equations relative to a particular model were derived.

Note that the V_{max}/U_{max0} ratio would give the rate constant k_{31} in the above model, which is not equivalent in the most general case to the turnover number of the carrier protein given by k_{cat} in Eq. (B7) unless $k_{31} \ll k_{12}$. Such considerations may also be model dependent.

References

1. Alvaradez-Hernandez, X., Nichols, G.M., Glass, J. 1991. Caco-2 cell line: a system for studying intestinal iron transport across epithelial cell monolayers. *Biochim. Biophys. Acta* **1070:**205–208
2. American Public Health Association, American Water Works Association, Water Pollution Control Federation. 1989. Methods 3111-B. *In:* Standard methods for the Examination of Water and Waste Water, 17th edition. L.S. Clesceri, A.E. Greenberg, and R. Rhodes Trussell, editors. Washington, DC
3. Anderson, O. 1984. Chelation of cadmium. *Environ. Health Perspect* **54:**249–266
4. Ando, M., Matsui, S. 1987. Effect of cadmium on vitamin D-non-stimulated intestinal calcium absorption in rats. *Toxicology* **45:**1–11
5. Barry, P.H., Diamond, J.M. 1984. Effects of unstirred layers on membrane phenomenon. *Physiol. Rev.* **64:**763–872
6. Beattie, J.H., Marion, M., Schmit, J.-P., Denizeau, F. 1990. The cytotoxic effects of cadmium chloride and mercuric chloride mixtures in rat primary hepatocyte cultures. *Toxicology* **62:**161–173
7. Blais, A., Bissonnette, P., Berteloot, A. 1987. Common characteristics for Na^+-dependent sugar transport in Caco-2 cells and human fetal colon. *J. Membrane Biol.* **99:**113–125
8. Blazka, M.E., Shaikh, Z.A. 1991. Differences in cadmium and mercury uptakes by hepatocytes: role of calcium. *Toxicol. Appl. Pharmacol.* **110:**355–363
9. Bradford, M.M. 1979. A rapid and sensitive method for the quantitation of microgram quantities of protein utilizing the principle of protein-dye binding. *Anal. Biochem.* **72:**248–254
10. Chantret, I., Rodolosse, A., Barbat, A., Dussaulx, E., Brot-Laroche, E., Zweibaum, A., Rousset, M. 1994. Differential expression of sucrase-isomaltase in clones isolated from early and late passages of the cell line Caco-2: evidence for glucose-dependent negative regulation. *J. Cell Sci.* **107:**213–225
11. Chenu, C., Berteloot, A. 1993. Allosterism and Na^+-D-Glucose cotransport kinetics in rabbit jejunal vesicles: compatibility with mixed positive and negative cooperativities in a homo-dimeric or tetrameric structure and experimental evidence for only one transport protein involved. *J. Membrane Biol.* **132:**95–113
12. Flanagan, J.L., Friedman, P.A. 1991. Parathyroid hormone-stimulated cadmium accumulation in Madin-Darby canine kidney cells. *Toxicol. Appl. Pharmacol.* **109:**241–250
13. Fogh, J., Fogh, J.M., Orfeo, T. 1977. One hundred and twenty seven cultured human tumor cell lines producing tumors in nude mice. *J. Natl. Canc. Inst.* **59:**221–226
14. Foulkes, E.C. 1980. Some determinants of intestinal cadmium transport in the rat. *J. Environ. Pathol. Toxicol.* **3:**471–481
15. Foulkes, E.C. 1985. Interaction between metals in rat jejunum: implications on the nature of cadmium uptake. *Toxicology* **37:**117–125
16. Friedman, P.A., Gesek, F.A. 1994. Cadmium uptake by kidney distal convoluted tubule cells. *Toxicol. Appl. Pharmacol.* **128:**257–263
17. Garty, M., Bracken, W.M., Klaassen, C.D. 1986. Cadmium uptake by rat blood cells. *Toxicology* **42:**111–119
18. Gerson, R.J., Shaikh, Z.A. 1984. Differences in the uptake of cad-

mium and mercury by rat hepatocyte primary cultures: role of a sulfhydryl carrier. *Biochem. Pharmacol.* **33:**199–203
19. Giuliano, A.R., Franceschi, R.T., Wood, R.J. 1991. Characterization of the vitamin D receptor from the Caco-2 human colon carcinoma cell line: effect of cellular differentiation. *Arch. Biochem. Biophys.* **285:**261–269
20. Goon, D., Klaassen, C.D. 1989. Dosage-dependent absorption of cadmium in the rat intestine measured in situ. *Toxicol. Appl. Pharmacol.* **100:**41–50
21. Grasset, E., Pinto, M., Dussaulx, E., Zweibaum, A., Desjeux, J.F. 1984. Epithelial properties of human colon carcinoma cell line Caco-2: Electrical parameters. *Am. J. Physiol.* **247:**C260–C267
22. Hamilton, D.L., Smith, M.W. 1978. Inhibition of intestinal calcium uptake by cadmium and the effect of a low calcium diet on cadmium retention. *Environ. Res.* **15:**175–184
23. Hoadley, J.E., Johnson, D.R. 1987. Effects of calcium on cadmium uptake and binding in the rat intestine. *Fund. Appl. Pharmacol.* **9:**1–9
24. Jaeger, D.E. 1990. Absorption interactions of zinc and cadmium in the isolated perfused rat intestine. *J. Trace Elem. Electrolytes Health Dis.* **4:**101–105
25. Jumarie, C., Herring-Gillam, E., Beaulieu, J.-F., Malo, C. 1996. Triiodothyronine stimulates the expression of sucrase-isomaltase in Caco-2 cells cultured in serum-free medium. *Exp. Cell Res.* **222:**319–325
26. Jumarie, C., Malo, C. 1991. Caco-2 cells cultured in serum-free medium as a model for the study of enterocytic differentiation in vitro. *J. Cell. Physiol.* **149:**24–33
27. Kello, D., Kostial, K. 1977. Influence of age and milk diet on cadmium absorption from the gut. *Toxicol. Appl. Pharmacol.* **40:**277–282
28. Khoo, C., Cousins, R.J. 1994. Purification and properties of rat cystein-rich intestinal protein. *Biochem. J.* **299:**445–450
29. Kimmich, G.A. 1990. Membrane potentials and mechanism of intestinal Na^+-dependent sugar transport. *J. Membrane Biol.* **114:**1–127
30. Kunst, A., Draeger, B., Ziegenhorn, J. 1984. UV-methods with hexokinase and glucose-6-phosphate deshydrogenase. *In:* Methods of enzymatic analysis, 3nd ed. H.U. Bergmeyer, editor. Vol. VI. Metabolites. 1: Carbohydrates, pp. 163–172. Verlag Chemies, Weinheim
31. Mahraoui, L., Rodolosse, A., Barbat, A., Dussaulx, E., Zweibaum, A., Rousset, M. 1994. Presence and differential expression of SGLT1, GLUT1, GLUT2, GLUT3 and GLUT5 hexose-transporter mRNAs in Caco-2 cell clones in relation to cell growth and glucose consumption. *Biochem. J.* **298:**629–633
32. Malo, C., Berteloot, A. 1991. Analysis of kinetic data in transport studies: new insights from kinetic studies of Na^+-D-glucose cotransport in human brush-border membrane vesicles using fast sampling, rapid filtration apparatus. *J. Membrane Biol.* **122:**127–141
33. Nriagu, J.O., Pacyna, J.M. 1988. Quantitative assessment of worldwide contamination of air, water and soils by trace metals. *Nature* **333:**134–139
34. Ohta, H., Cherian, M.G. 1991. Gastrointestinal absorption of cadmium and metallothionein. *Toxicol. Appl. Pharmacol.* **107:**63–72
35. Pinto, M., Robine-Leon, S., Appray, M.D., Kedinger, M., Triadou, N., Dussaulx, E., Lacroix, B., Simon-Assman, P., Haffen, K., Fogh, J., Zweibaum, A. 1983. Enterocytic-like differentiation and polarization of the human colon carcinoma cell line Caco-2 in culture. *Biol. Cell* **47:**323–330
36. Raffaniello, R.D., Lee, S.-Y., Teichberg, S., Wapnir, R.A. 1992. Distinct mechanism of zinc uptake at the apical and basolateral membranes of Caco-2 cells. *J. Cell. Physiol.* **152:**356–361
37. Robards, K., Worsfold, P. 1991. Cadmium: toxicology and analysis, a review. *Analyst* **116:**549–568
38. Rousset, M., Laburthe, M., Pinto, M., Chevalier, G., Rouyer-Fessard, C., Dussaulx, E., Trugnan, G., Boige, N., Brun, J.L., Zweibaum, A. 1985. Enterocytic differentiation and glucose utilization in the human colon tumor cell line Caco-2: Modulation by forskolin. *J. Cell. Physiol.* **123:**377–385
39. Segel, I.H. 1975. Steady-state kinetics of multireactant enzymes. *In:* Enzyme kinetics. J. Wiley & Sons, editors. Chap. 9, pp. 505–845. Wiley-Interscience, USA
40. Shaikh, Z.A., Smith, J.C. 1980. Metabolism of orally ingested cadmium in humans. *Develop. Toxicol. Environ. Sci.* **8:**569–574
41. Sharma, G., Sandhir, R., Nath, R., Gill, K. 1991. Effect of ethanol on cadmium uptake and metabolism of zinc and copper in rats exposed to cadmium. *J. Nutr.* **121:**87–91
42. Sowa, B., Steibert, E. 1985. Effect of oral cadmium administration to female rats during pregnancy on zinc, copper, and iron content in placenta, foetal liver, kidney, intestine, and brain. *Arch. Toxicol.* **56:**256–262
43. Sugawara, N. 1977. Inhibitory effect of cadmium on calcium absorption from the rat duodenum. *Arch. Environ. Contam. Toxicol.* **5:**167–175
44. Tacnet, F., Watkins, D.W., Ripoche, P. 1990. Studies of zinc transport into brush-border membrane vesicles isolated from pig small intestine. *Biochim. Biophys. Acta* **1024:**323–330
45. Tsien, R.W., Hess, P., McCleskey, E.W., Rosenberg, R.L. 1987. Calcium channels: mechanisms of selectivity, permeation and block. *Ann. Rev. Biophys. Chem.* **16:**265–290
46. Tsuruki, F., Otawara, Y., Wung, H.L., Moriuchi, S., Hosoya, N. 1978. Inhibitory effect of cadmium on vitamin D-stimulated calcium transport in rat duodenum in vitro. *J. Nutr. Sci. Vitaminol.* **24:**237–242
47. Van Os, C.H. 1987. Transcellular calcium transport in intestinal and renal epithelial cells. *Biochim. Biophys. Acta* **906:**195–222
48. Verbost, P.M., Senden, M.H.M.N., Van Os, C.H. 1987. Nanomolar concentrations of Cd^{2+} inhibit Ca^{2+} transport systems in plasma membrane and intracellular Ca^{2+} stores in intestinal epithelium. *Biochim. Biophys. Acta* **902:**247–252
49. Waalkes, M.P. 1986. Effect of dietary zinc deficiency on the accumulation of cadmium and metallothionein in selected tissues of the rat. *J. Toxicol. Environ. Health* **18:**301–313
50. Wohlhueter, R.M., Plagemann, P., G., W. 1980. The roles of transport and phosphorylation in nutrient uptake in cultured animal cells. *Int. Rev. Cytol.* **64:**171–240
51. Yuhas, E.M., Miya, T.S., Schnel, R.C. 1978. Influence of cadmium on calcium absorption from the rat intestine. *Toxicol. Appl. Pharmacol.* **43:**23–31